REPORT No. 651

DOWNWASH AND WAKE BEHIND PLAIN AND FLAPPED AIRFOILS

By Abe Silverstein, S. Katzoff and W. Kenneth Bullivant

SUMMARY

Extensive experimental measurements have been made of the downwash angles and the wake characteristics behind airfoils with and without flaps and the data have been analyzed and correlated with the theory. A detailed study was made of the errors involved in applying lifting-line theory, such as the effects of a finite wing chord, the rolling-up of the trailing vortex sheet, and the wake.

The downwash angles, as computed from the theoretical span load distribution by means of the Biot-Savart equation, were found to be in satisfactory agreement with the experimental results. The rolling-up of the trailing vortex sheet may be neglected, but the vertical displacement of the vortex sheet requires consideration.

By the use of a theoretical treatment indicated by Prandtl, it has been possible to generalize the available experimental results so that predictions can be made of the important wake parameters in terms of the distance behind the airfoil trailing edge and the profile-drag coefficient.

The method of application of the theory to design and the satisfactory agreement between predicted and experimental results when applied to an airplane are demonstrated.

INTRODUCTION

Rational tail-plane design depends on a knowledge of the direction and the velocity of the air flow in the region behind the wing. Numerous investigations, both experimental and theoretical, have been devoted to the determination of the downwash for wings without flaps. The agreement between theory and experiment has, as a rule, been only partly satisfactory, and the comparisons have been inadequate as bases for generalizations. The existing empirical equations for downwash angles make allowance neither for variations in plan form nor for the use of flaps. Only scant attention has been given to the important problem of the wake behind flapped wings.

As the first part of a comprehensive study of tail-plane design, the air flow in the region behind the wing has been studied for the purpose of developing general methods for predicting the downwash and the wake. Much of the work on downwash was concerned with the relation of the induced field in the region behind the airfoil to the theoretical span load distribution and to the corresponding vortex system. The basis for the theoretical calculations is the Biot-Savart equation for the induced velocities in a vortex field. Some of the data were particularly useful in investigating the rate of rolling-up of the trailing vortex sheet.

The wake constitutes a not altogether separate problem. Its position and the velocity distribution across it must be known in order to predict the tail efficiency for cases in which the tail is within it. Downwash and wake generally require simultaneous treatment because the downwash determines the position of the wake and the wake has, in turn, an effect on the downwash.

The data used in this analysis were obtained mainly in the N. A. C. A. full-scale wind tunnel with airfoils and airplanes that were usually so small that the jet-boundary corrections either were negligible or could be accurately applied.

An obvious limitation of the present study, insofar as its practical utility is concerned, lies in its neglect of the interference from fuselage, nacelles, etc. Also neglected is the small effect of the tail itself on the air flow ahead of it.

EXPERIMENTAL INVESTIGATION

SCOPE OF THE TESTS

The airfoils, the airplane model, and the full-scale airplane used in the investigation, together with a synopsis of the downwash and the wake surveys made in each case, are listed as follows:

1. A 5- by 30-inch rectangular Clark Y airfoil. Downwash angles were measured, at three different lift coefficients, in the plane of symmetry. Dynamic-pressure surveys of the wake were made in the same plane.

2. A 10- by 30-inch rectangular Clark Y airfoil. Measurements were the same as for the 5- by 30-inch airfoil.

3. A 2- by 12-foot rectangular Clark Y airfoil tested without a flap, and with the following flaps, each of 20-percent chord:

(a) 40-percent-span split flap, $\delta_f=20°$ and 60°.

(b) 70-percent-span split flap, $\delta_f=20°$ and 60°.

(c) Same as (b) except for a 12.5-percent-span cutaway at the center.

(d) Full-span split flap, $\delta_f=20°$ and 60°.

(e) Full-span external-airfoil flap, $\delta_f=20°$ and 40°.

Downwash measurements were made, at three lift coefficients, in the plane of symmetry of the airfoil and also in a parallel plane one-sixth of the span from the symmetry plane.

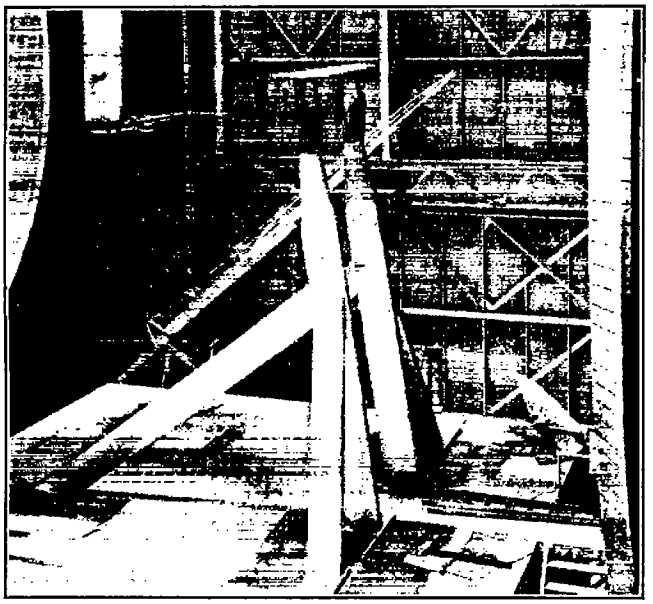

FIGURE 1.—The U. S. A. 45 airfoil mounted in the full-scale wind tunnel and the survey apparatus behind it.

4. The 45.75-foot-span, 2:1 tapered U. S. A. 45 airfoil of aspect ratio 6 described in reference 1. Downwash and wake measurements were made at five lift coefficients, in the plane of symmetry, and in planes 3, 8, 18, 21, and 24 feet from the symmetry plane at distances of 10, 18, and 26 feet behind the quarter-chord point.

5. A model of 12-foot span of the 2:1 tapered U. S. A. 45 airfoil. Downwash measurements were similar to those for the 2- by 12-foot rectangular airfoil.

6. The 8- by 48-foot rectangular Clark Y airfoil described in reference 2. Downwash and wake surveys were similar to those for the large U. S. A. 45 tapered airfoil.

7. Three 6- by 36-foot symmetrical airfoils of N. A. C. A. 0009, 0012, and 0018 sections. Detailed measurements of the wake were made at a number of longitudinal stations from the trailing edge to three chord lengths behind the airfoils.

8. A small low-wing monoplane equipped with a 5:1 tapered wing of aspect ratio 10. The wing has a plain sealed flap extending over 65 percent of the span. Downwash and wake measurements were made with the tail removed, in the region of the tail plane for a number of different lift coefficients with and without the flap deflected.

9. A midwing airplane model equipped with a 4:1 tapered wing of aspect ratio 8. The wing has a split flap extending over 58 percent of the span. Downwash and wake measurements were made in the region of the tail plane. Pitching-moment measurements were also made with the tail at different settings and with the tail removed.

APPARATUS AND METHODS

The experimental work was conducted in the N. A. C. A. full-scale wind tunnel (reference 3) using the survey apparatus that is part of the equipment of the tunnel. Figure 1, showing the survey apparatus behind the 12-foot U. S. A. 45 airfoil, illustrates the experimental arrangement. For the 5- by 30-inch and the 10- by 30-inch airfoils, the measurements were made with a small Y-type yaw head and a Prandtl pitot tube, as described in detail in reference 4. For all other cases, the measurements were obtained by means of the combined pitch, yaw, and dynamic-pressure tube shown in detail in figure 2. Force measurements were made by the methods described in references 2, 3, and 4.

Angles of pitch and yaw are accurate to within about ±0.25°. Dynamic-pressure measurements are accurate to within about ±1 percent.

Air-stream angles and dynamic pressures were measured without an airfoil in the jet, and these values were applied in correcting all the measurements. Jet-boundary corrections were negligible for the two small Clark Y airfoils. Corrections were applied according to reference 4 for the airfoils of 12-foot span and for the two airplanes. For the large airfoils, the corrections are so large and vary so much from point to point in the region behind the airfoil that a quantitative comparison between the theoretical and the measured downwash angles was not considered advisable.

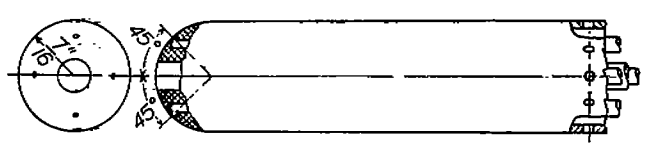

FIGURE 2.—Line drawing showing combined pitch, yaw, and pitot-static tube used for the dynamic-pressure and the downwash surveys.

CALCULATION OF DOWNWASH

The induced velocity at a point due to an infinitesimal length of vortex filament is given by the Biot-Savart equation, which may be written in vector notation

$$\bar{w}=\frac{\Gamma}{4\pi}\frac{d\bar{l}\times\bar{a}}{|\bar{a}|^3}$$

in which $\bar{w}$ is the induced-velocity vector at the point.

Γ, the strength of the vortex.

$d\bar{l}$, a vector having the direction and length of the infinitesimal vortex filament.

$\bar{a}$, the vector from the vortex filament to the point.

The integration of this expression around a semi-infinite U-vortex of semispan s and strength Γ, in order to obtain the effect at a point x, z in the symmetry plane, leads to the following expressions for the separate contributions to the vertical component of the induced velocity at this point.

$$w_1=\frac{s\Gamma}{2\pi}\frac{x}{(x^2+z^2)\sqrt{s^2+x^2+z^2}}$$

due to the bound vortex.

$$w_2=\frac{s\Gamma}{2\pi}\frac{1}{s^2+z^2}\left(1+\frac{x}{\sqrt{s^2+x^2+z^2}}\right)$$

due to the two trailing vortices.

$$w_1+w_2=w=\frac{s\Gamma}{2\pi}\left[\frac{x}{\sqrt{s^2+x^2+z^2}}\left(\frac{1}{x^2+z^2}+\frac{1}{s^2+z^2}\right)+\frac{1}{s^2+z^2}\right] \quad (1)$$

due to the U-vortex.

By means of equation (1) a computation of the downwash angle behind a monoplane airfoil can be made if the load distribution, or circulation distribution, along the airfoil is known. The wing is replaced by its lifting line, where the bound vortex is considered localized, and the vortex sheet that is shed from its trailing edge is considered to originate at the lifting line and extend, unchanged, to infinity. The strength Γ of the bound vortex at any section is related to the section lift coefficient c_l by the equation

$$\Gamma=\frac{Vcc_l}{2}$$

in which V is the free-stream velocity and c is the chord length. The intensity of vorticity in the trailing vortex sheet is $-d\Gamma/dy$.

In a separate paper (reference 5) are presented, for use in tail-plane design and stability studies, the results of extensive downwash computations based on the foregoing idealized picture. These computations being for wings of various aspect ratios, taper ratios, and flap spans, it is essential to investigate the generality of the method and to justify its application.

The validity of the foregoing concept as a foundation for the computation of downwash angles is, indeed, subject to objection in a number of particulars, which have been separately studied and are discussed in the following sections. The cases of wings without and with flaps are separately treated.

WINGS WITHOUT FLAPS

Flow about an airfoil section.—An obvious objection to the proposed method of calculation is that a vortex at the lifting line is an inexact substitution for the actual airfoil. In order to investigate the order of magnitude of the discrepancy, the theoretical two-dimensional flow about a Clark Y airfoil at $C_L=1.22$ was obtained by a conformal transformation of the

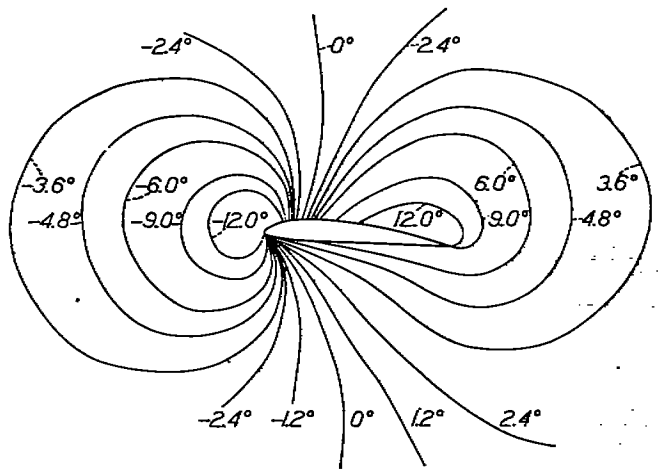

FIGURE 3.—Theoretical downwash-angle contours for two-dimensional flow about a Clark Y airfoil section. α, 5.43°; C_L, 1.22.

flow about a circle. The transformation was effected by the method of Theodorsen (reference 6); the Clark Y airfoil was chosen because much of the experimental work was done with Clark Y airfoils and also because the transformation had already been partly performed

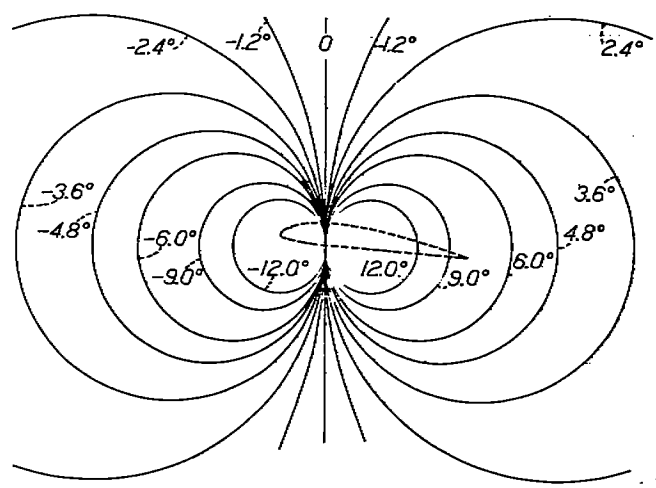

FIGURE 4.—Theoretical downwash-angle contours for a vortex in a uniform stream (two-dimensional flow). Vortex strength corresponds to $C_L=1.22$.

in reference 6 for this section. Four complex Fourier coefficients were used, which, inasmuch as they sufficed to transform the circle with good accuracy into the Clark Y section, necessarily sufficed to transform the flow at distances from it.

The results are plotted as downwash-angle contours in figure 3. Comparison with the corresponding map for an equivalent vortex placed at the quarter-chord point (fig. 4) shows that, at a distance of about one chord length behind the trailing edge, the difference is less than 0.3°. It appears reasonable to assume that the difference would be of this order for other airfoils.

The conclusiveness of this result may be open to question inasmuch as the actual flow about an airfoil section only approximates the potential flow, owing to the finite viscosity of air; the difference is probably

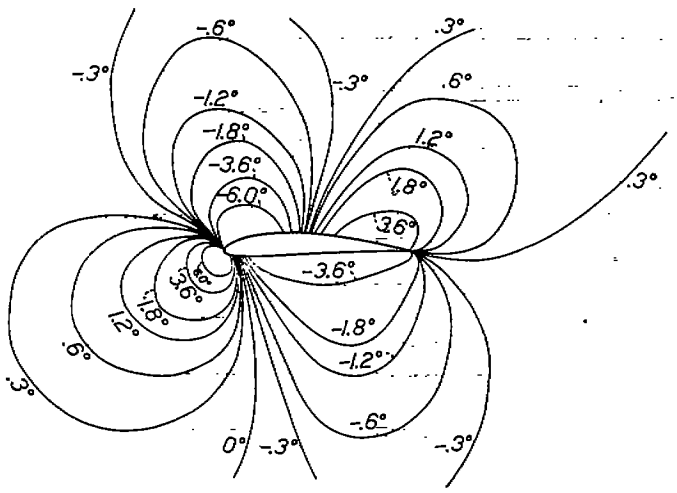

FIGURE 5.—Theoretical downwash-angle contours for two-dimensional flow about a Clark Y airfoil section. α, −5.57°; C_L, 0.

slight, however, except in the vicinity of the wake itself.

Figure 5 shows the theoretical stream angles calculated for the Clark Y airfoil at zero lift. The simplified theory for this case predicts zero downwash at every point in the field; and it can be seen that, at one chord length behind the trailing edge, the difference from zero is small.

Distortion of the trailing vortex sheet.—The shed vortex sheet does not extend unaltered indefinitely downstream but, as a result of the air motions that the vortex system itself creates, is rapidly displaced down-

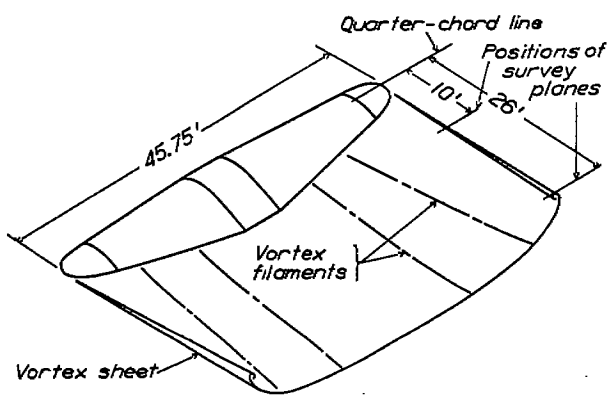

FIGURE 6.—Isometric drawing showing the U. S. A. 45 airfoil and the distorted trailing vortex sheet. C_L, 1.35.

ward and deformed. It curves into a channel of constantly increasing depth and distends rapidly as it proceeds to roll up like a volute about the tip-vortex cores.

It is essential to know the rate at which this transformation occurs, for the difference in the tail-plane region between the downwash computed for the unchanged vortex sheet and that for the completely rolled-up sheet is of the order of 20 percent. The surveys behind the large U. S. A. 45 tapered airfoil are of particular interest in this respect, because they were sufficiently extensive to give quantitative information on the rolling-up process. For this purpose, the case of the highest lift coefficient (C_L=1.35) will be discussed, not only because the greater magnitude of the measured pitch and yaw angles increases the relative accuracy of the study but also because the distortion of the vortex sheet at the rearmost survey plane (26 feet behind the quarter-chord line) represents the maximum distortion that will have to be considered in practical computations of downwash behind plain wings. The bases for this statement are: (a) the aspect ratio is about the minimum in common use; (b) the lift coefficient is quite high, in fact, nearly the maximum for this airfoil; and (c) the 26-foot survey plane is considerably farther

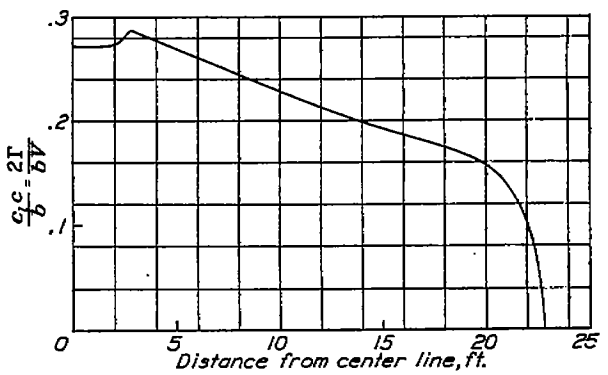

FIGURE 7.—Experimental span load distribution for the U. S. A. 45 airfoil. C_L, 1.35.

behind the trailing edge than is the usual position of the tail plane.

Figure 6 shows the shape of the airfoil and the positions of the 10-foot and the 26-foot survey planes. Figure 7 shows the span load distribution for C_L=1.35, experimentally determined by means of pressure orifices in the airfoil surface (reference 1). Figures 8 and 9 show the surveys in the 10-foot and the 26-foot planes, respectively, the vectors representing by magnitude and direction the inclination of the air flow to the tunnel axis. In order to avoid confusion, vectors are not shown for all points where readings were taken.

The line of intersection of the trailing vortex sheet with the plane of the survey has been indicated in the figures; it is the line across which there is an abrupt change in the lateral component of the velocity. It is also the line where the wake intersects the survey plane, as was verified by the dynamic-pressure surveys. The circles indicating the positions of the tip-vortex cores are somewhat more arbitrarily located; they are points that appear to be the approximate centers of rotation of the air flow near them.

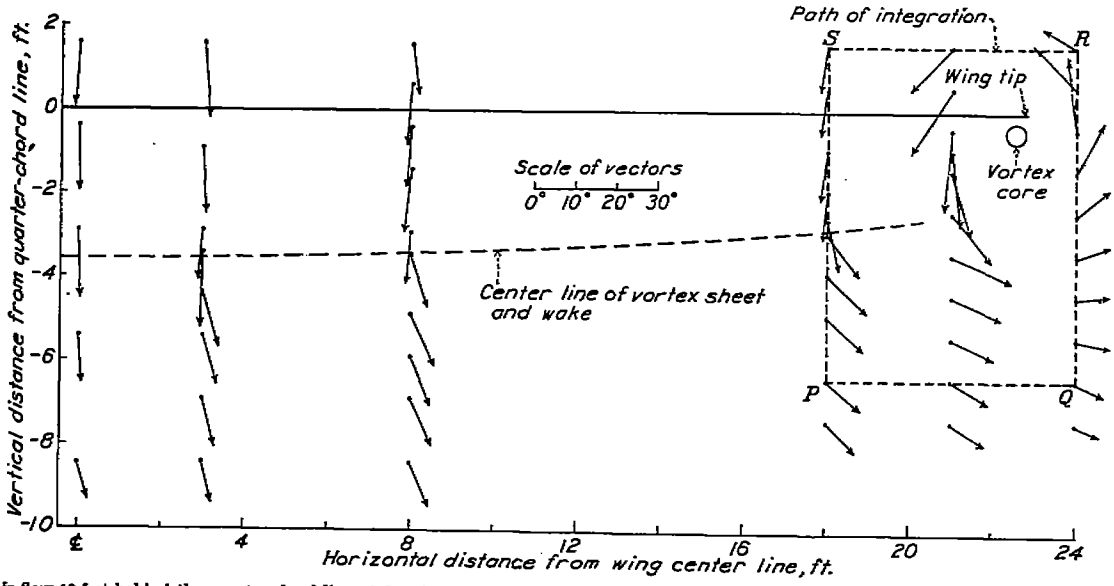

FIGURE 8.—Air flow 10 feet behind the quarter-chord line of the U. S. A. 45 tapered airfoil. Vectors denote deviation of air flow from free-stream direction. C_L, 1.35.

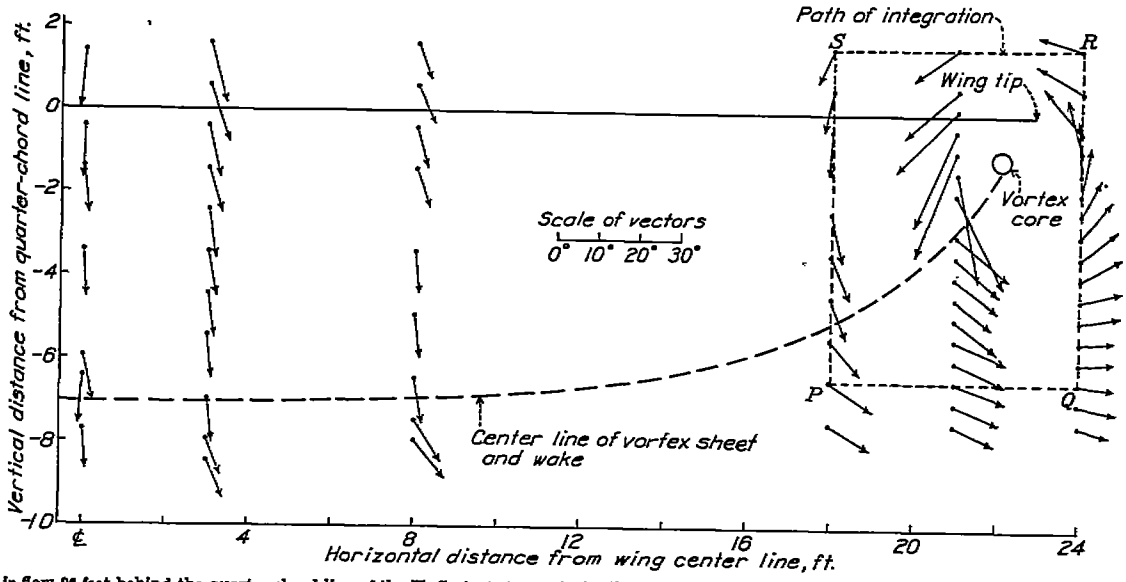

FIGURE 9.—Air flow 26 feet behind the quarter-chord line of the U. S. A. 45 tapered airfoil. Vectors denote deviation of air flow from free-stream direction. C_L, 1.35.

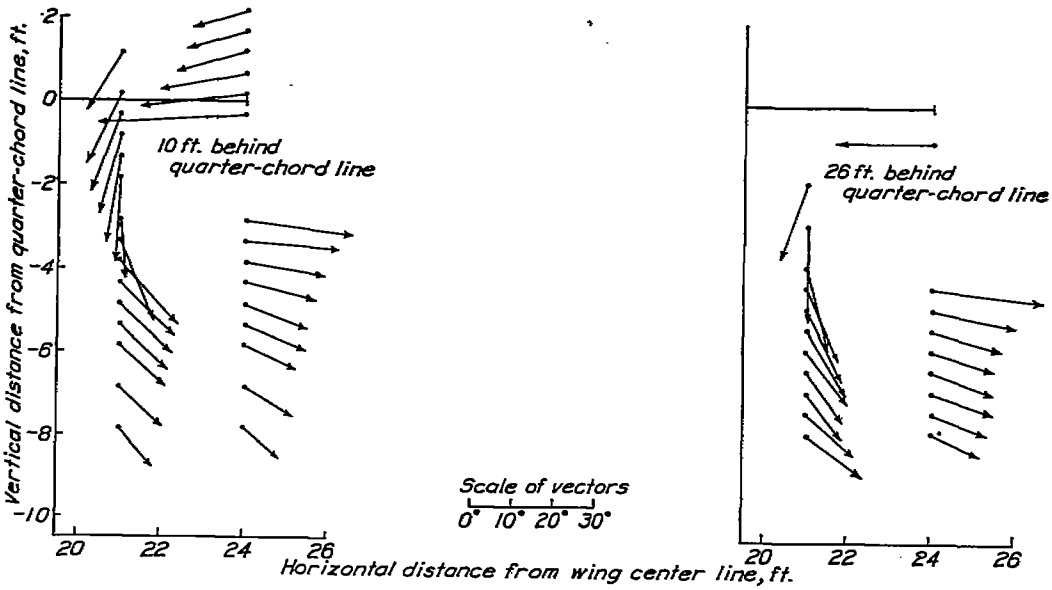

FIGURE 10.—Air flow behind the tip of the 8- by 48-foot Clark Y airfoil. Vectors denote deviation of air flow from free-stream direction. C_L, 1.44.

Rolling-up of the trailing vortex sheet.—It was possible to determine from the surveys the extent of rolling-up of the sheet at each survey plane. From Stokes' theorem, the total strength of the vorticity Γ within an area S may be determined by integrating the tangential component of the velocity along the boundary C of the area. Thus, in the usual vector notation,

$$\Gamma=\int_S\int \text{curl } \overline{V}\cdot d\overline{A}=\oint_C \overline{V}\cdot d\overline{r}$$

where $d\overline{A}$ and $d\overline{r}$ are, respectively, vector elements of area and of boundary, and $\overline{V}$ is the velocity vector.

Now, the circulation around the airfoil at, say, 18 feet from the center is known from the experimental span load distribution and the air speed. This circulation constitutes the amount of vorticity that must be shed from the trailing edge between this point and the airfoil tip. If the trailing vortex sheet extended unchanged indefinitely downstream, the value of $\oint \overline{V}\cdot d\overline{r}$ along any path that enclosed the edge of the sheet and cut the sheet 18 feet from the center, as, for example, the path $SPQR$ in figure 9, should equal this circulation. Owing to the rolling-up, however, the amount of vorticity within such a path exceeds this amount, especially when the point at which the path cuts the sheet is well back of the trailing edge. The excess indicates the extent of the rolling-up.

Such integrations were performed along the rectangular paths shown in figures 8 and 9. The integration along these paths is particularly simple, for, along the vertical sides, $\overline{V}\cdot d\overline{r}=V \sin \theta \, dr$ and, along the horizontal sides, $\overline{V}\cdot d\overline{r}=V \sin \psi \, dr$, where θ and ψ are the experimentally determined pitch and yaw angles, V is the local air speed, and dr is the length of the path element.

From these integrations it was found that, at 10 feet behind the quarter-chord line, the total vorticity in the area of integration was 1.024 as much as the circulation around the airfoil at the 18-foot station; whereas, at 26 feet behind the quarter-chord line, it was 1.13 as much. These values correspond, respectively, to the circulations that existed on the airfoil at 17.2 feet and 14.3 feet from the center. It follows that the vortex sheet leaving the trailing edge rolls up at such a rate that, in the first survey plane, the vorticity originally between 17.2 feet and the edge has all been concentrated between 18 feet and the tip; and, in the rear survey plane, the part originally outboard of 14.3 feet has been concentrated between 18 feet and the tip. Integrations about the inner parts of the vortex sheet showed, as expected, that the inner part lost as much vorticity as the tip gained.

The rest of the sheet must distend correspondingly. Thus, the portion extending originally between the center and 14.3 feet from the center has, at the 26-foot survey plane, become so distended that it reaches to 18 feet. Further evidence on this distention is found in the surveys made in the vertical line 8 feet from the center (figs. 8 and 9). The rate of outward displacement of the vortex filaments 8 feet from the center is roughly given by the average of the yaw angles just above and just below the sheet. At the 10-foot and the 26-foot survey planes, these average angles are 2.5° and 3.5°, respectively. The mean along the path being thus about 3° and the length of the path being about 19 feet, it follows that a vortex filament leaving the trailing edge 8 feet from the center has moved out to about $8+19 \tan 3°=9$ feet from the center by the time it reaches the rearmost survey plane. The paths of this filament, the filament leaving the trailing edge 14.3 feet from the center, and the tip-vortex core have been indicated in figure 6. The surveys in the symmetry plane and in the line 3 feet from it are of uncertain interpretation, because the pressure-orifice measurements showed anomalous lift distribution near the center of the airfoil.

It may be remarked that, although the distortion and distention found are not inconsiderable, the rolling-up process, by which the vorticity is eventually concentrated into a pair of tip vortices, appears to be still far from complete. This result is evident from the position of the tip-vortex core, located at the approximate center of rotation of the air flow near the tip. It has moved in only to 96 percent of the semispan whereas, for complete rolling-up, it would be at 78 percent of the semispan. Figure 10 shows similar surveys behind the tip of the 8- by 48-foot Clark Y airfoil. For complete rolling-up, the tip vortex would be at about 87 percent of the semispan, whereas the survey shows it almost at the tip.

Further evidence of the displacement of the tip-vortex core is found in the photographs obtained in smoke-flow studies and reproduced in figure 11. The visible flows were obtained with kerosene vapor flowing past the tip of the tapered half-wing mounted on a reflecting board. The core of the tip vortex is easily discerned as far back in the mouth of the exit bell as can be seen, a total distance of about 50 feet. This visual method was not capable of yielding quantitative results although, qualitatively, it was clear that the inward displacement of the tip-vortex core was small.

Kaden's theoretical calculations (reference 7) indicate that the rolling-up process is not complete until a distance of $0.56A/C_L$ semispans behind the trailing edge of the airfoil. For a lift coefficient C_L of 1.35 and an aspect ratio A of 6, this value is 2.5 semispans, or about four times as far back as is the usual location of the tail. It may be remarked that, in Muttray's work (reference 8), the rolling-up, as determined by the inward displacement of the tip-vortex core, was found to be slower than is given by the foregoing expression.

The effect of rolling-up on the downwash.—It will be recalled that, in the tentative scheme for calculating downwash angles, the trailing vortex sheet is assumed to originate at the lifting line and to extend unchanged to infinity. The question now arises as to how seriously such rolling-up, distortion, and distention of the trailing vortex sheet as were found in the preceding study affect the accuracy of the results computed on this basis. For purposes of comparison, calculations were made of the downwash angles in the symmetry plane at a distance of 1.15 semispans behind the quarter-chord line (corresponding to the rearmost survey plane behind the U. S. A. 45 airfoil) using the theoretical span load distribution for a 2:1 tapered airfoil of aspect ratio 6, for the following cases (fig. 12):

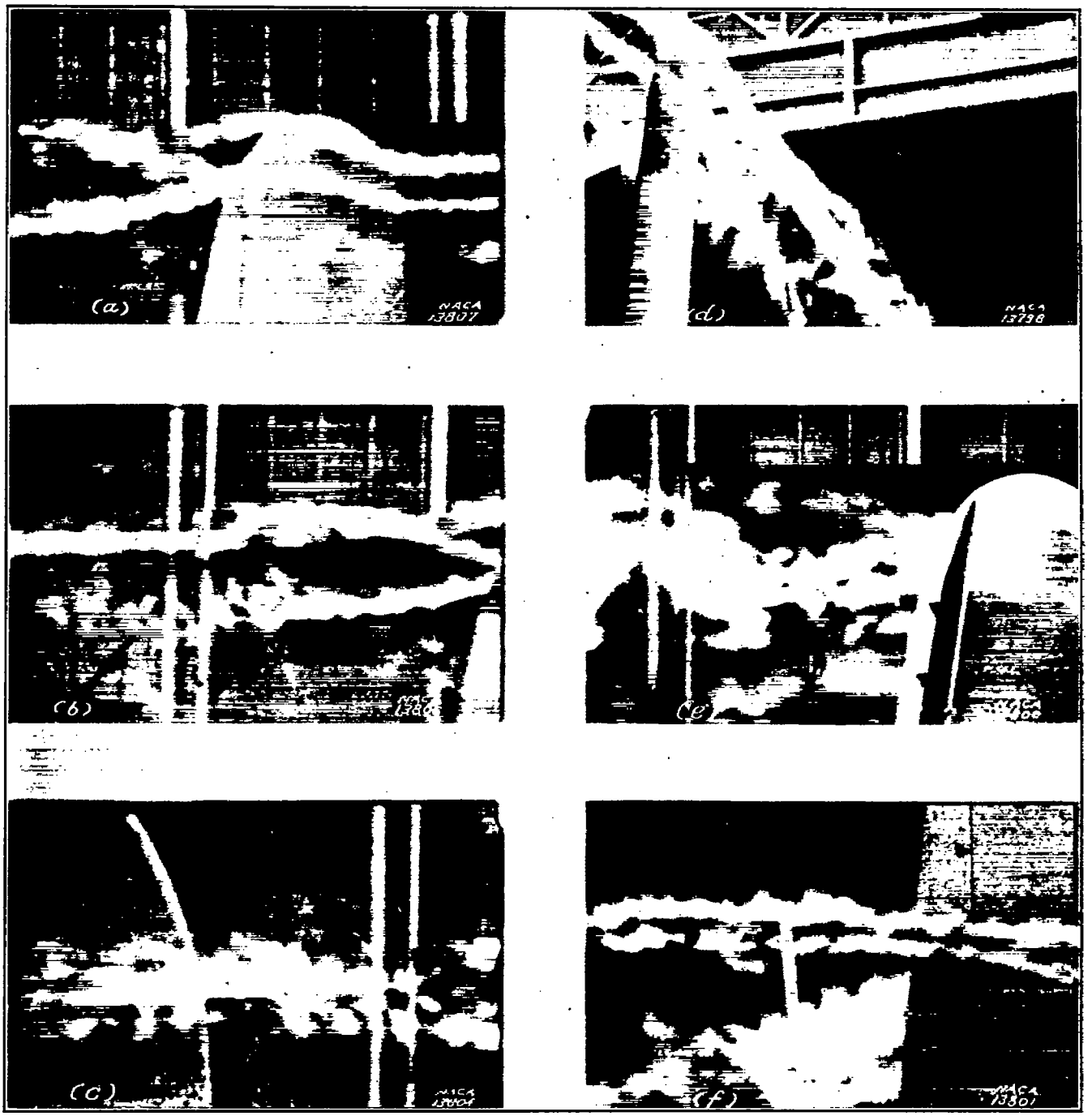

(a), (b), (c), (d)—Views showing tip vortex core forming at wing tips and moving downstream. Plain wing without flap.
(e)—View of flow at tip of the wing with 0.20c full-span split flap deflected 60°. (f)—View showing flow at the tip of a partial-span split flap.

FIGURE 11.—Smoke-flow pictures for the U. S. A. 45 tapered airfoil in the full-scale wind tunnel. Wing vertical.

(a) The vortex sheet assumed to be distorted and rolled up to the same extent as found at the rearmost survey plane in the foregoing study and to exist in this state from the wing to infinity. The actual vortex sheet, of course, is distorted less than this amount ahead of this position and more than this amount behind this position. It is very difficult to take this variation into account in the calculations, however, and the error involved in assuming the distortion to be uniform appears to be negligible.

(b) The vortex sheet assumed to be neither distorted nor rolled up but to extend straight behind the quarter-chord line to infinity.

The curves in figure 12 show the corresponding downwash angles, calculated for $C_L=1.35$, plotted against vertical distance from the level of the quarter-chord line. The curve for b is distinctly separate from that for a. Most of the difference, however, consists of a relative vertical displacement. Thus, curve c, which is the same as b but shifted vertically by an amount equal to the displacement of the center of the curved sheet, does not differ from that for a by more than 1° in the region of interest and differs from it hardly at all at small distances above the wake. For low-wing or midwing monoplanes, the tail will usually be at small distances above the wake and the downwash computed as for c will therefore, for these cases, correspond to the actual distorted vortex sheet. Furthermore, it will be recalled that the present example is very nearly a limiting, if not an exaggerated case; for the more usual conditions, the distortion will be much less, and the difference between a and c will be negligible.

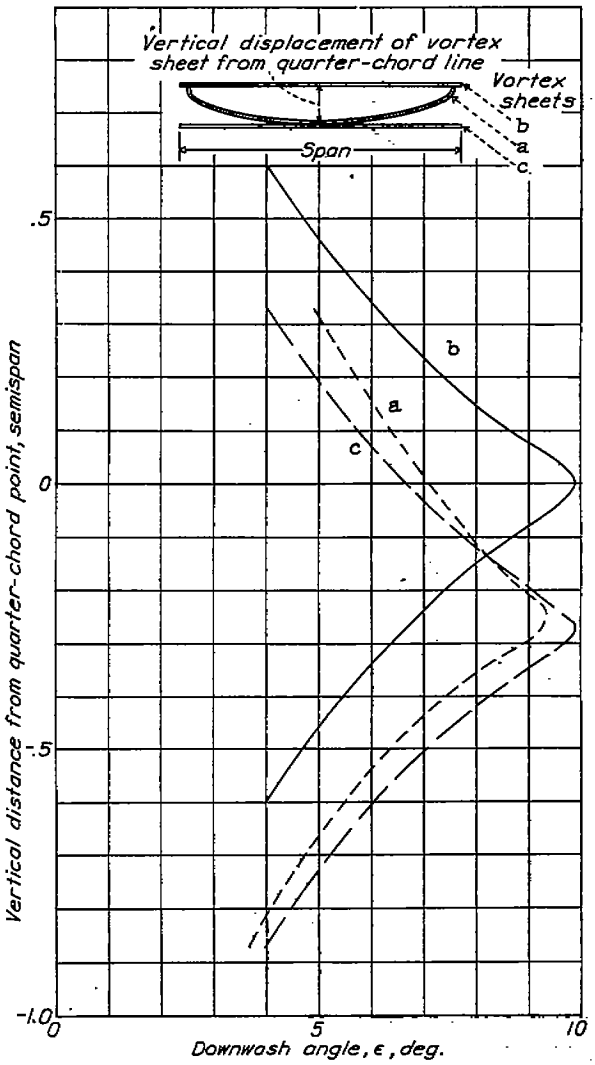

FIGURE 12.—Calculated downwash for the plane of symmetry, 1.15 semispans behind the quarter-chord line of a 2:1 tapered airfoil of aspect ratio 6. C_L, 1.35. a, Vortex sheet distorted as found for the U. S. A. 45 tapered airfoil; b, Vortex sheet assumed to extend unchanged straight behind the quarter-chord line to infinity; c, same as b, but displaced vertically by an amount equal to the displacement at the middle of the distorted sheet.

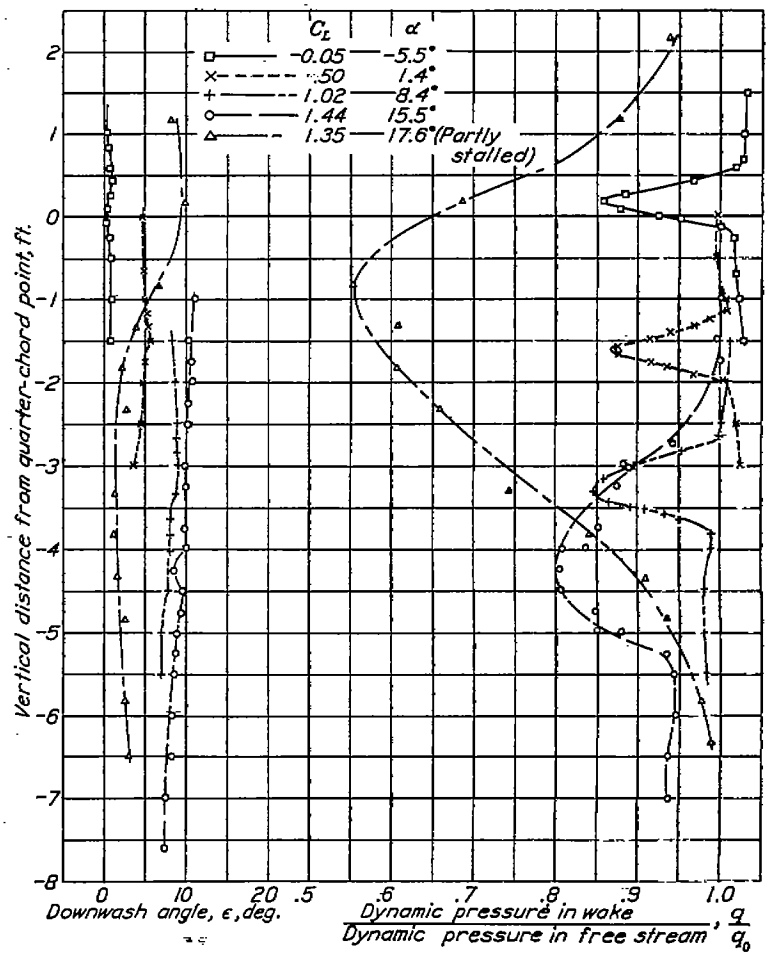

FIGURE 13.—Downwash-angle and dynamic-pressure surveys in the symmetry plane 18 feet behind the quarter-chord line of the 8- by 48-foot Clark Y airfoil.

The following conclusion is thus reached: In the computation of downwash angles behind plain airfoils, it is usually sufficiently accurate to neglect the distention of the vortex sheet and to take into account the distortion simply by considering the entire vortex sheet to be displaced vertically by an amount equal to the displacement of the center line of the actual distorted sheet. This displacement, in turn, is readily calculated, for the center line passes through the trailing edge and moves

downward with the downwash itself. Its inclination at every point is the downwash angle ϵ at that point; hence the vertical displacement from the trailing edge is given simply by the expression

$$\int_{T.E.}^{x} \tan \epsilon \, dx$$

Influence of the wake.—The wake, which is the rearward extension of the boundary layer and which

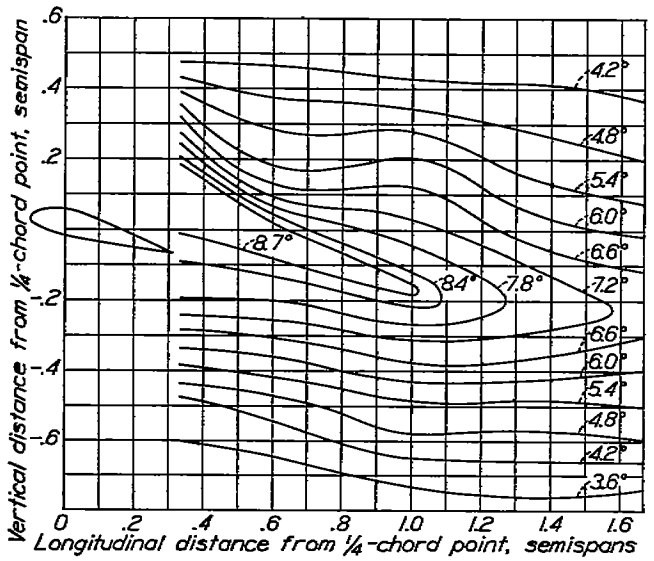

FIGURE 14.—Downwash-angle contours in the symmetry plane behind the 12-foot U. S. A. 45 tapered airfoil. α, 11.5°; C_L, 1.175.

coincides with the trailing vortex sheet, affects the motion of the air in its vicinity. There is a flow of air toward the wake center, as will be obvious on considering that the velocity in the wake increases with distance from the trailing edge, requiring that the stream lines converge. The effect therefore consists of an increase in the downwash above the wake and a decrease in the downwash below it.

Some indication as to the magnitude of the effect for airfoils without flaps may be obtained from the surveys made in the symmetry plane behind the 8- by 48-foot Clark Y airfoil. The dynamic pressures and the downwash angles in the wake region are plotted in figure 13 for five different lift coefficients. The effect at the two lowest lift coefficients is too small to be detected. At the next two lift coefficients (C_L=1.02 and 1.44), the downwash above the wake exceeds that below it; but no quantitative information on the wake effect can be obtained from these data, because the distortion of the vortex sheet also contributes a disymmetry of the same order of magnitude. The curve for the partly stalled wing (C_L=1.35) shows an effect amounting to several degrees.

Theoretical calculations of the wake effect on downwash based on the wake description presented in a later section of this report have been made. They indicate, in agreement with these data, that the maximum effect of the wake on the downwash angle at the tail is about 0.2° for unstalled plain wings. For wings with high-drag flaps or for partly stalled wings, the effect may be ten times as great. Details of these calculations will be given after the discussion of the wake equations.

Sweepback and dihedral.—Wings with sweepback introduce some complication into the theory, since the component vortices for such a case do not have the simple rectangular U-shape. Some computations made for a wing with a normal amount of sweepback showed the effect to be much too small to require consideration. The lifting line may therefore be assumed to be perpendicular to the symmetry plane and to pass through the quarter-chord point of the root section.

Dihedral has an indirect effect on the downwash in that it gives the trailing vortex sheet an initial distortion which, however, is usually small. Thus, for the U. S. A. 45 tapered airfoil, the shed vortex sheet leaves the trailing edge with an initial dihedral of about 3.5°, thereby

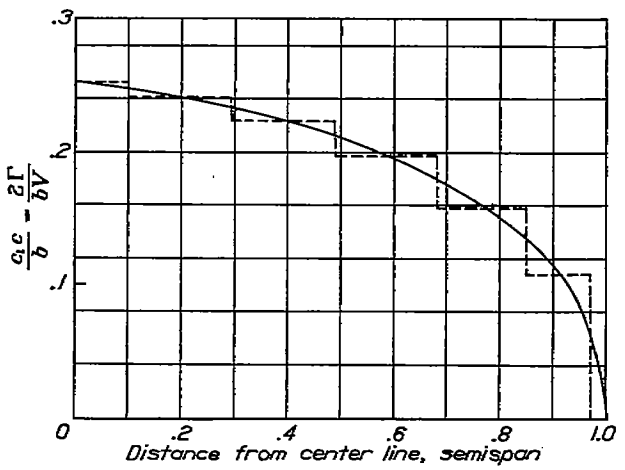

FIGURE 15.—Theoretical span load distribution for the 12-foot U. S. A. 45 tapered airfoil and the equivalent stepwise distribution used in the downwash calculations. C_L, 1.175.

contributing only about one-fifth of the total distortion found in the rearmost survey plane.

Span load distribution.—It may be pointed out that, in order to carry out a computation of the downwash angles, it will usually be necessary to use the theoretical span load distribution as derived, for example, by the method of Glauert (reference 9) or of Lotz (reference 10). The theoretical span load distribution thus derived corresponds closely to the actual distribution, provided that the airfoil has a reasonably high aspect ratio and rounded tips, although its accuracy in the neighborhood of discontinuities in either chord or angle is questionable.

Sample calculation of downwash and comparison with experiment.—It may be desirable to illustrate by an example the computation of the downwash angles behind an airfoil and to show, by comparison with experiment, the accuracy of the results. The experimental downwash-angle contour map (fig. 14) for the 12-foot tapered airfoil at C_L=1.175 was chosen for the comparison.

For the theoretical curve of span load distribution (fig. 15), an approximately equivalent, stepwise dis-

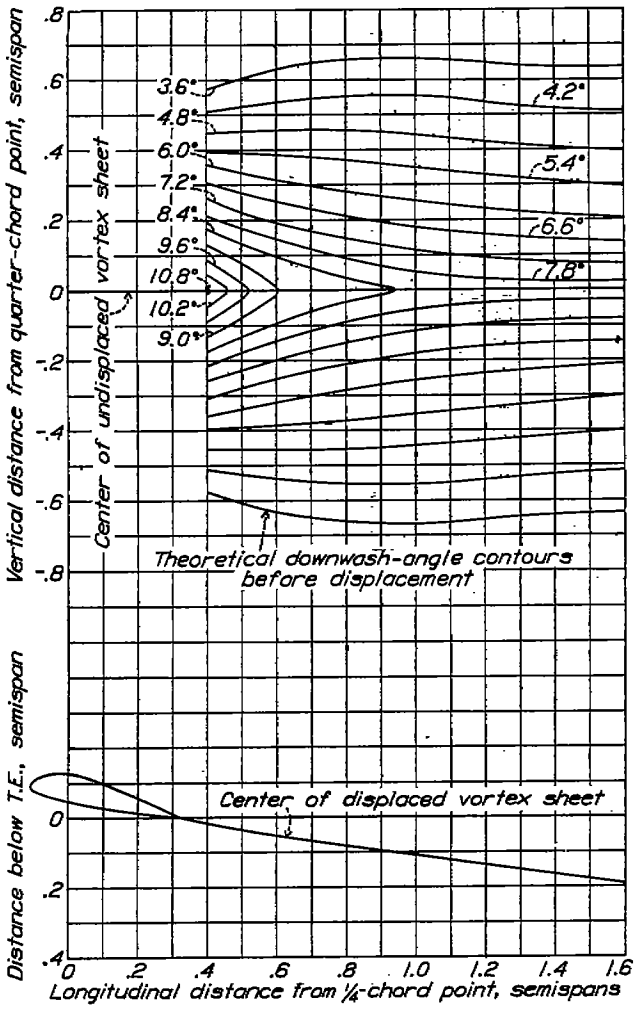

FIGURE 16.—Theoretical undisplaced downwash-angle contours and the center of the displaced vortex sheet. The 12-foot U. S. A. 45 tapered airfoil. C_L, 1.175.

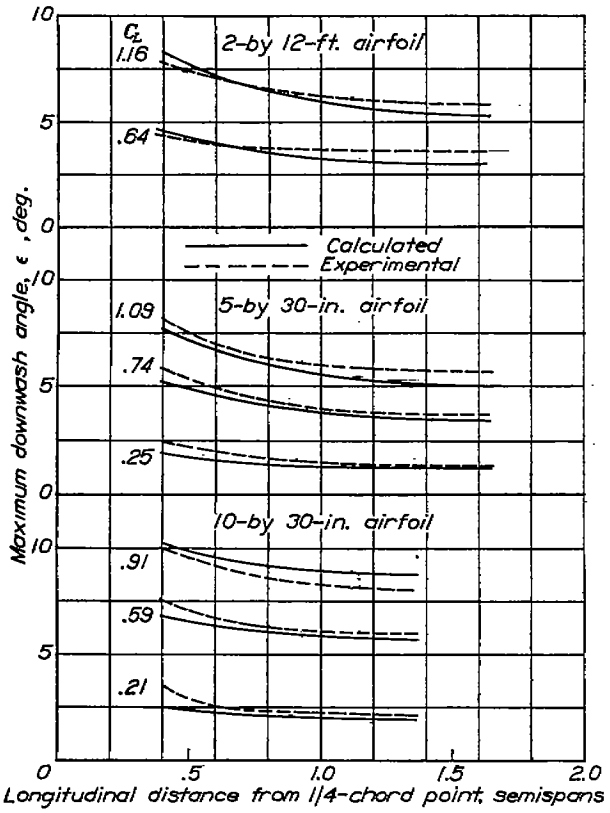

FIGURE 18.—Comparison of calculated and experimental maximum downwash-angles behind rectangular airfoils.

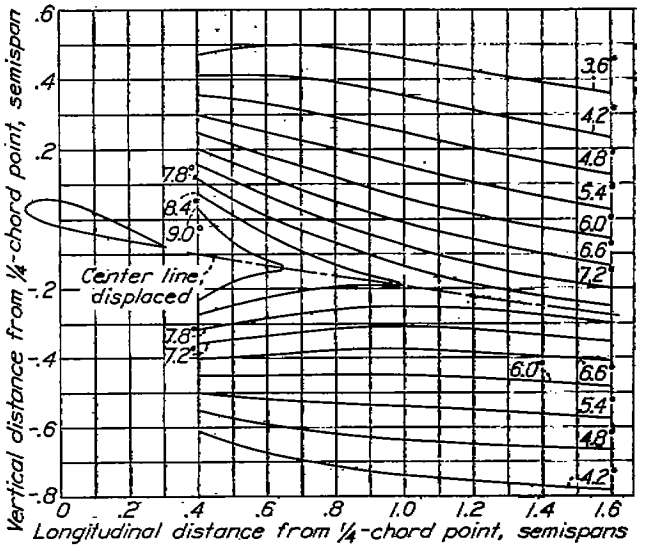

FIGURE 17.—Theoretical displaced downwash-angle contours in the symmetry plane of the 12-foot U. S. A. 45 tapered airfoil. C_L, 1.175.

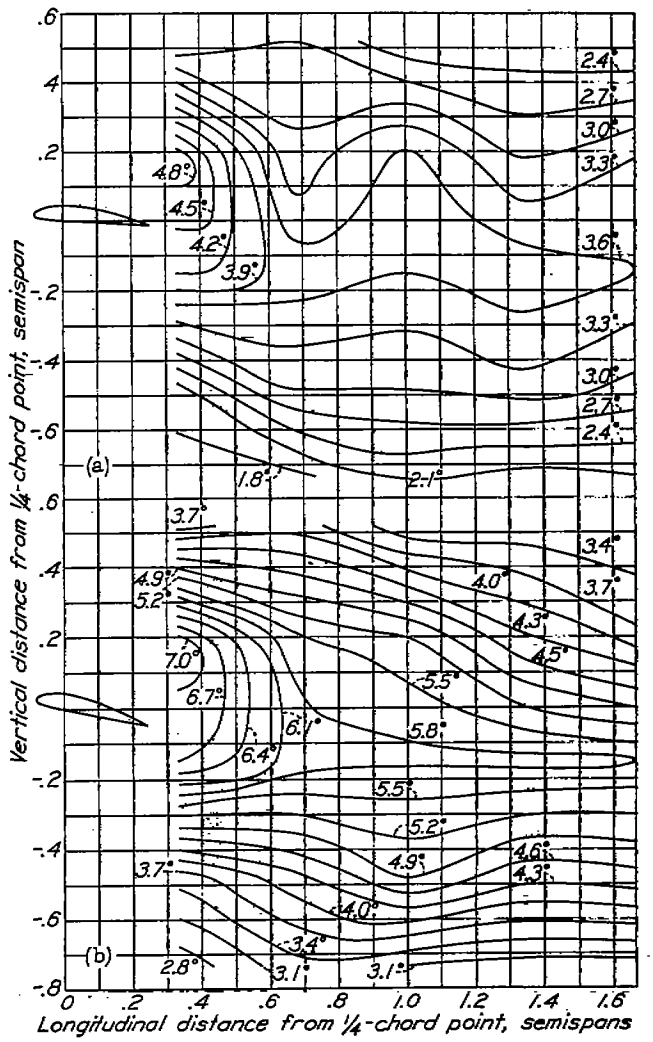

(a) C_L=0.64.
(b) C_L=1.16.

FIGURE 19.—Downwash-angle contours in the symmetry plane of the 2- by 12-foot Clark Y airfoil.

tribution is substituted. A vortex of strength given by the amount of the rise is considered to be shed at each step, and the downwash angles are computed for points in the symmetry plane by means of equation (1).

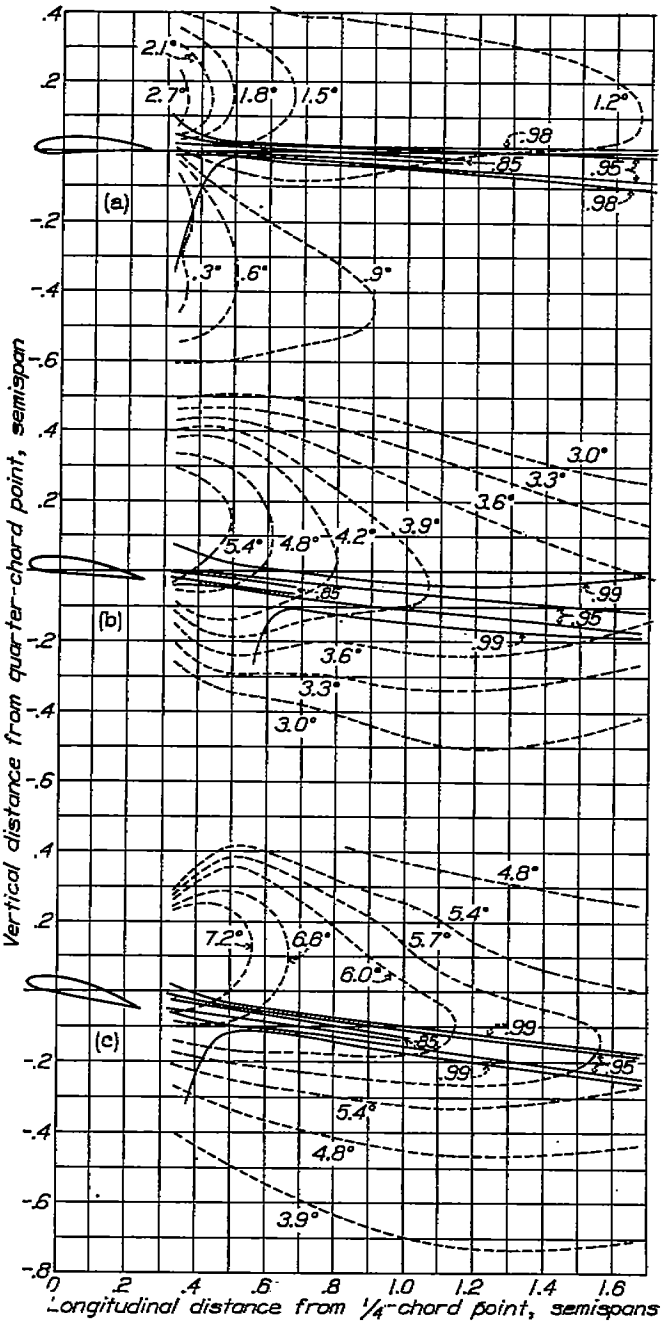

(a) $\alpha=-3.8°$; $C_L=0.25$.
(b) $\alpha=3.2°$; $C_L=0.74$.
(c) $\alpha=9.2°$; $C_L=1.09$.

FIGURE 20.—Downwash-angle and dynamic-pressure contours in the symmetry plane of the 5- by 30-inch Clark Y airfoil. Dynamic pressures are shown as fractions of free-stream dynamic pressure.

It is assumed here that the trailing vortices extend unchanged indefinitely downstream. The resulting downwash-angle contour map is shown in figure 16. Distorting this map so that the center line goes through the trailing edge and has, at every point, an inclination equal to the downwash angle at that point, leads to the map of figure 17, which is now to be compared with the experimental map (fig. 14). It will be seen that the agreement is, on the whole, satisfactory, particularly in the region where the tail plane is usually located, namely, about 0.75 semispan back. The following discrepancies may be noted:

1. The theoretical downwash angle approaches 7.8° on the center line at large distances, whereas the experimental downwash angle has already dropped to 7° at two semispans back and appears to be still decreasing rapidly with distance. This difference, as was shown by computation, is due to the distortion of the vortex sheet into a channel, the depth of which is about 0.4 semispan. It may be remarked that, for complete rolling-up, with the two halves of the trailing vortex sheet concentrated at their centroids, the downwash angle would be 5.0° in this region.

2. There is a dissymmetry in the experimental downwash map at the farther distances behind the airfoil

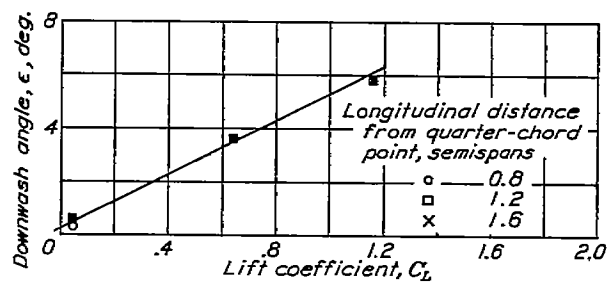

FIGURE 21.—Variation of maximum downwash angle in the symmetry plane with C_L for the 2- by 12-foot Clark Y airfoil.

in that the angles decrease faster below the maximum than above it. This dissymmetry is also due to the deformation of the sheet, as may be seen by referring to curve a of figure 12.

3. There is a region of large downwash angles above the center line, just behind the airfoil. This characteristic is predicted by airfoil-section theory and may be observed, for example, in the theoretical flow about the Clark Y section (fig. 3).

Other less complete comparisons between theoretical and experimental downwash angles are given in figure 18, where the maximum theoretical and experimental downwash angles are plotted against longitudinal position. The agreement is satisfactory, although the experimental downwash angles are somewhat larger than the theoretical except where the distortion and the rolling-up of the vortex sheet become considerable, as for the 10- by 30-inch airfoil at $C_L=0.91$. Figure 19 shows experimental downwash-angle contour maps for the 2- by 12-foot airfoil at two lift coefficients. Figure 20 shows similar contour maps for the 5- by 30-inch airfoil and also shows the wake. This figure is of particular interest, for it shows clearly that the downwash maxima lie slightly above the wake.

If it is assumed that, for a wing without twist, the span load distributions (or circulation distribution) are similar at all angles of attack, it follows that downwash should be proportional to the lift coefficient. Examples of the proportionality between downwash and lift coefficient are shown in figure 21.

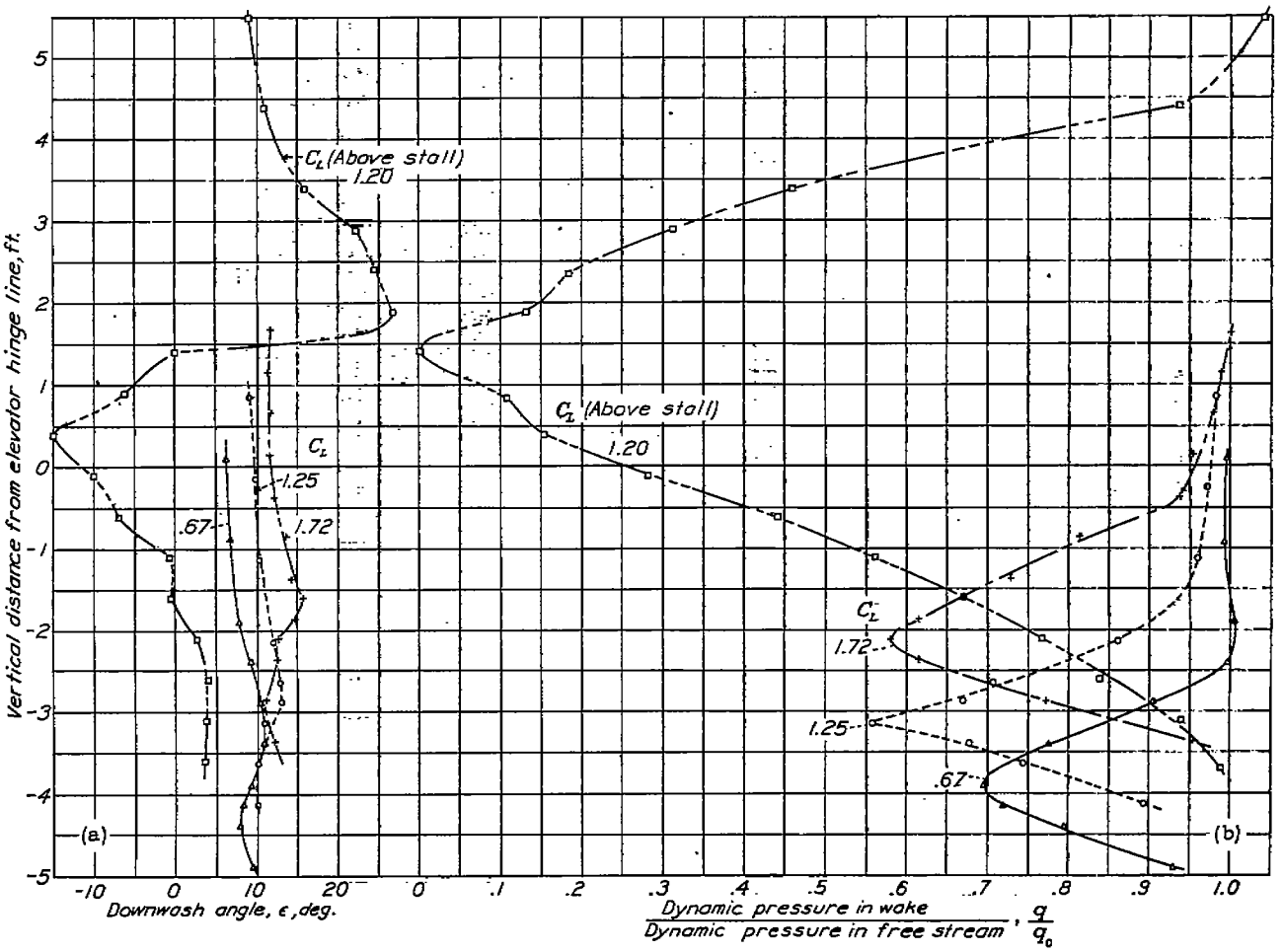

(a) Downwash angles. (b) Dynamic pressures.

FIGURE 22.—Downwash angles and dynamic pressures in the plane of the elevator hinge, 0.1 span from the symmetry plane. Low-wing monoplane with 65-percent-span plain flap deflected 45°.

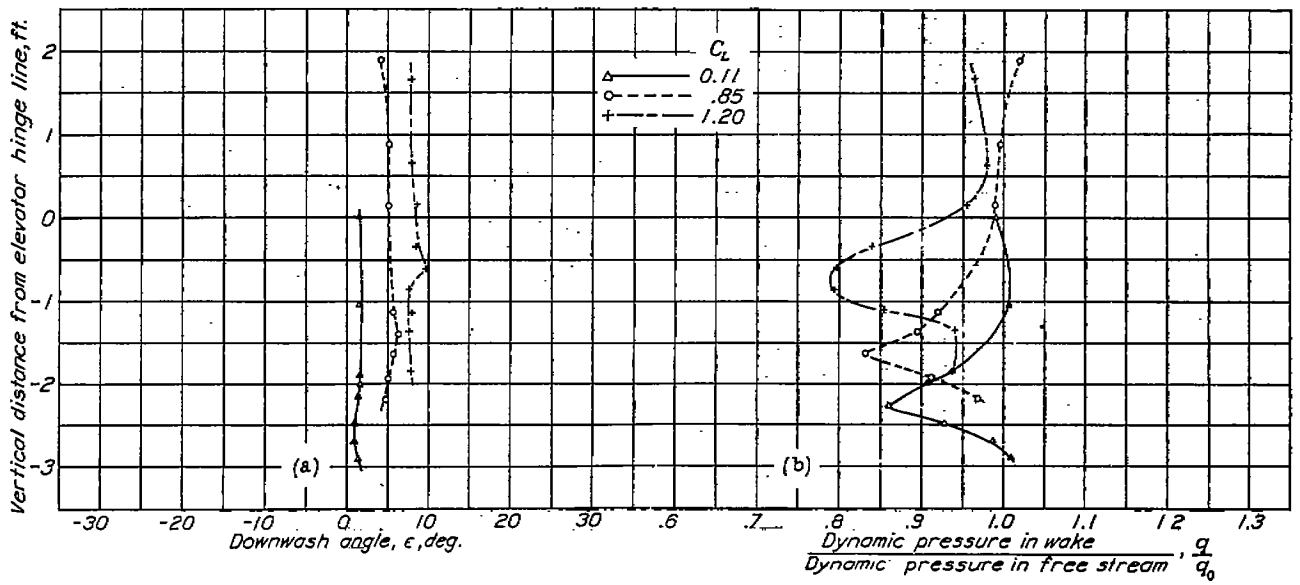

(a) Downwash angles. (b) Dynamic pressures.

FIGURE 23.—Downwash angles and dynamic pressures in the plane of the elevator hinge, 0.1 span from the symmetry plane. Low-wing monoplane with flap up.

WINGS WITH FLAPS

Provided that the span load distribution is known, the downwash may be computed for a flapped wing just as for a plain wing. It must be recognized, however, that the inaccuracies discussed in the preceding sections, which were concluded to have relatively small effect for plain wings, here acquire increased importance.

The wake, in particular, is many times stronger than that for a plain wing, and its effect in increasing the downwash angles near its upper border and decreasing them near its lower border is much more pronounced. Figure 22 shows the wake profiles and the corresponding

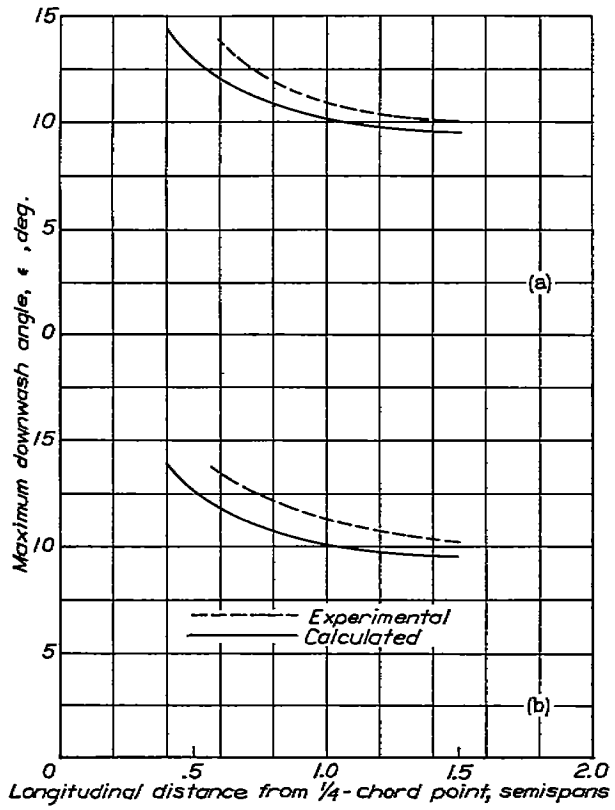

(a) External-airfoil flap deflected 20°; C_L, 2.08.
(b) Split flap deflected 60°; C_L, 2.01.

FIGURE 24.—Comparison of experimental with calculated maximum downwash behind the 2- by 12-foot Clark Y airfoil with full-span flaps.

downwash-angle plots in the plane of the elevator hinge line behind the low-wing monoplane with flaps down. The effect mentioned is seen to be considerable near the middle of the wake but is small outside the wake. For comparison, similar plots for the wing with flaps up are shown in figure 23.

In figure 24, the maximum theoretical and experimental downwash angles are plotted against longitudinal position for two cases of the 2- by 12-foot airfoil with full-span flaps. The excess of the experimental over the theoretical maximum downwash is approximately accounted for by the wake effect, as will be shown in a later section of this report. The experimental downwash-angle contour maps for these two cases are given in figures 25 and 26.

The deformation of the trailing vortex sheet for the case of partial-span flaps is also much more extensive than for the plain wing. Such distortion is indicated by the survey shown in figure 27, made in the vertical plane containing the elevator hinge line, behind the low-wing monoplane with flaps down. The trailing vortex sheet has been swept down sharply between the flap tip and the center. The origin of this peculiar deformation will be obvious on considering the direction of rotation of the flap-tip and the wing-tip vortices.

Data with which to study separately the foregoing influences are limited, and an exhaustive discussion of their effects is therefore not warranted. It appears likely, in view of the study for the plain wing, that no large discrepancy need be expected between the actual downwash angles and those computed by the previously described method, unless the flap span is inordinately small.

Calculation of downwash angles.—The theoretical downwash angles may be computed by the method that was given for plain wings, using the theoretical span load distribution, which, in these cases, consists of two parts, that for the plain wing and that for the flap. The flap contributions were calculated by the method of reference 10, sufficient data from lift measurements being available in each case to furnish the variables needed for the computation.

It may be desirable to state more explicitly the basis for the computation of the downwash increments due to flaps. The relative change in lift distribution on lowering a flap is nearly independent of the angle of attack, and the absolute change in the section lift coefficient c_l at any section is approximately proportional to the total increase in the wing lift coefficient C_{L_f}. The resultant loading and the resultant vortex system are therefore the sums of those of the plain wing at the given angle of attack and those due to the flap, which are proportional to C_{L_f}. The resulting downwash is, correspondingly, the sum of that of the plain wing at the given attitude and that due to the flap, the flap component again being proportional to C_{L_f}. The vertical displacement of the center line of the downwash-angle pattern is similarly additive.

In these span-loading calculations, the Fourier coefficients for the chord distribution were found by Pearson's system (reference 11) and the Fourier coefficients for the angle distribution were found by the usual method of integration. Ten terms of the series for the loading were used except in the case of the flap with the center cutaway, for which 20 terms were used. A reasonable number of terms does not suffice to give the shape of the loading curve very close to the edge of a flap; the curve is therefore more or less arbitrarily drawn in this region, the main condition being that it be vertical at the position of the flap tip.

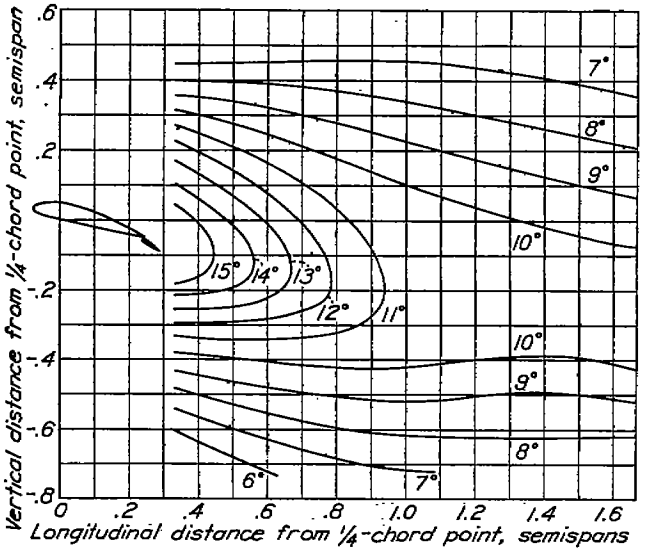

FIGURE 25.—Experimental downwash-angle contours in the symmetry plane behind the 2- by 12-foot Clark Y airfoil with full-span external-airfoil flap. δ_f, 20°; C_L, 2.08.

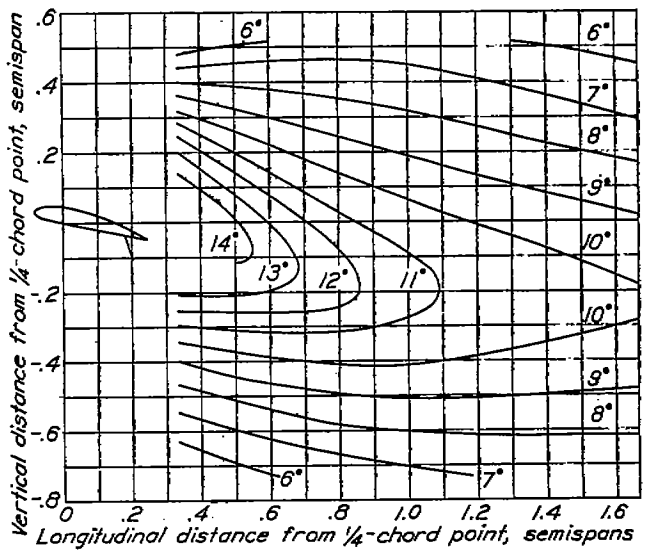

FIGURE 26.—Experimental downwash-angle contours in the symmetry plane behind the 2- by 12-foot Clark Y airfoil with full-span split flap. δ_f, 60°; C_L, 2.01.

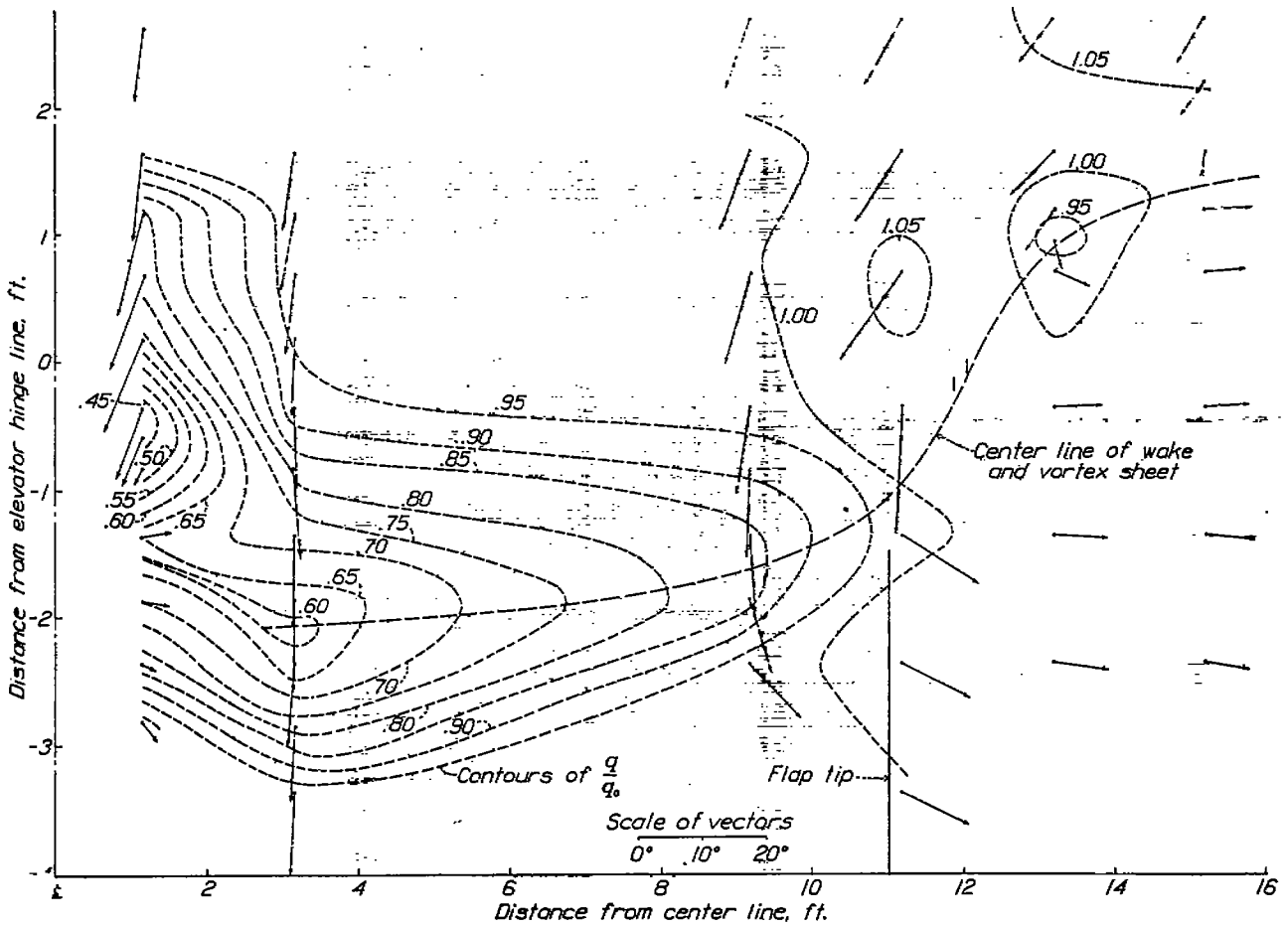

FIGURE 27.—Dynamic pressure and direction of air flow in the vertical plane through the elevator hinge. Vectors denote deviation of air flow from free-stream direction. Dynamic pressures in fractions of the free-stream dynamic pressure. Low-wing monoplane; 65-percent-span plain flap; δ_f, 45°; C_L, 1.725; α, 11.1°. Note that the vertical scale is twice the horizontal.

Sample calculation for flapped wings and comparison with experiments.—Figures 28 to 30 illustrate steps in the downwash-angle calculation for the case of the 2- by 12-foot airfoil with 70-percent-span split flap at $C_L=1.85$. The lift coefficient consists of two parts, $C_{L_w}=1.16$ and $C_{L_f}=0.69$; the corresponding two contributions to the span load distribution are shown in figure 28. The corresponding downwash-angle patterns, neglecting distortion or displacement of the shed

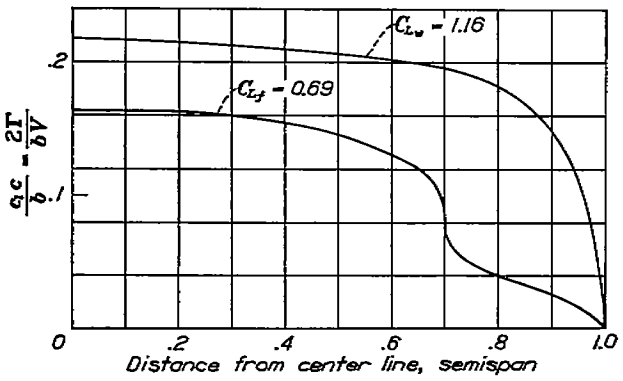

FIGURE 28.—Contributions of plain wing and of flap to span load distribution on the 2- by 12-foot Clark Y airfoil with 70-percent-span split flap. δ_f, 60°; C_{L_w}, 1.16; C_{L_f}, 0.69.

vortex sheet, are shown in figure 29. Adding these two contour maps and shifting the center line so that its inclination equals the downwash angle at every point gives the contour map shown in figure 30, which is now to be compared with the experimental downwash-angle contour map shown in figure 31 (a). The disagreement between the two is not large and is quantitatively attributable to the wake effects, as will appear later.

Figure 31 contains experimental downwash-angle contour maps, in the symmetry planes, for the 2- by 12-foot airfoil with 40-percent-span and 70-percent-span split flaps and with the 70-percent-span split flap having a 12.5-percent-span cutaway at the center. In figure 32, the maximum downwash angle is plotted against the longitudinal position and compared with the computed values. The difference between the experimental and the theoretical values may be ascribed to two effects: that of the wake, which increases the downwash; and that of the rolling-up, which, although insignificant for plain wings, appreciably reduces the downwash for short-span flaps. Thus, for the 70-percent flap, the first effect predominates (fig. 32 (a)); whereas, for the 40-percent flap at the higher lift coefficient, the second effect predominates (fig. 32 (c)).

A discrepancy of the order of 4° exists in the case of the 70-percent flap with the cutaway at the center. Agreement can hardly be expected, however, for there is little justification in using the lifting-line theory to calculate the span load distribution near a cutaway that is smaller than the wing chord or in assuming that the vortex sheet shed from the region of the cut-

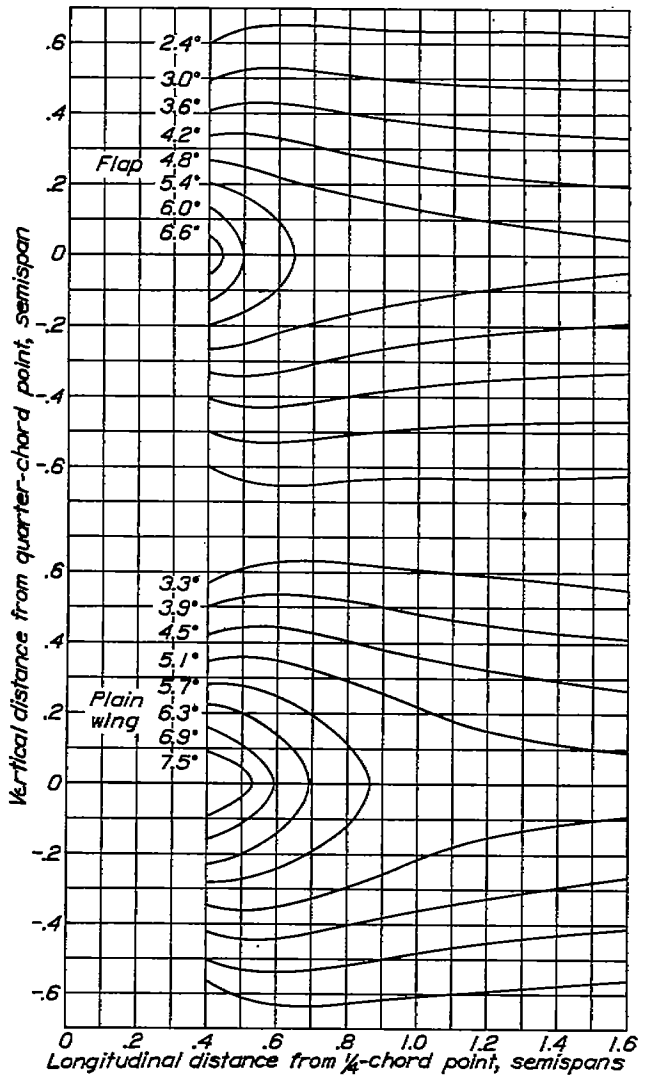

FIGURE 29.—Theoretical undisplaced downwash-angle contours, representing contributions of plain wing and of flap, for the 2- by 12-foot Clark Y airfoil with 70-percent-span split flap. δ_f, 60°; C_{L_w}, 1.16; C_{L_f}, 0.69.

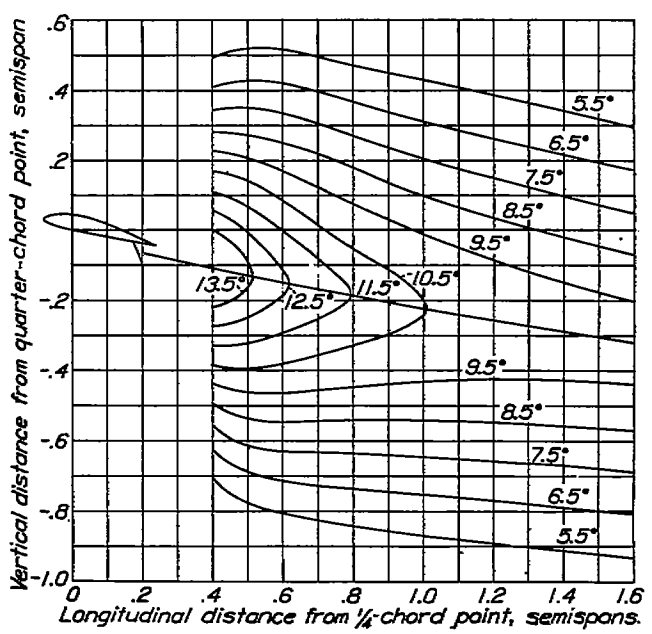

FIGURE 30.—Theoretical displaced downwash-angle contours for the 2- by 12-foot Clark Y airfoil with 70-percent-span split flap. δ_f, 60°; C_{L_w}, 1.16; C_{L_f}, 0.69.

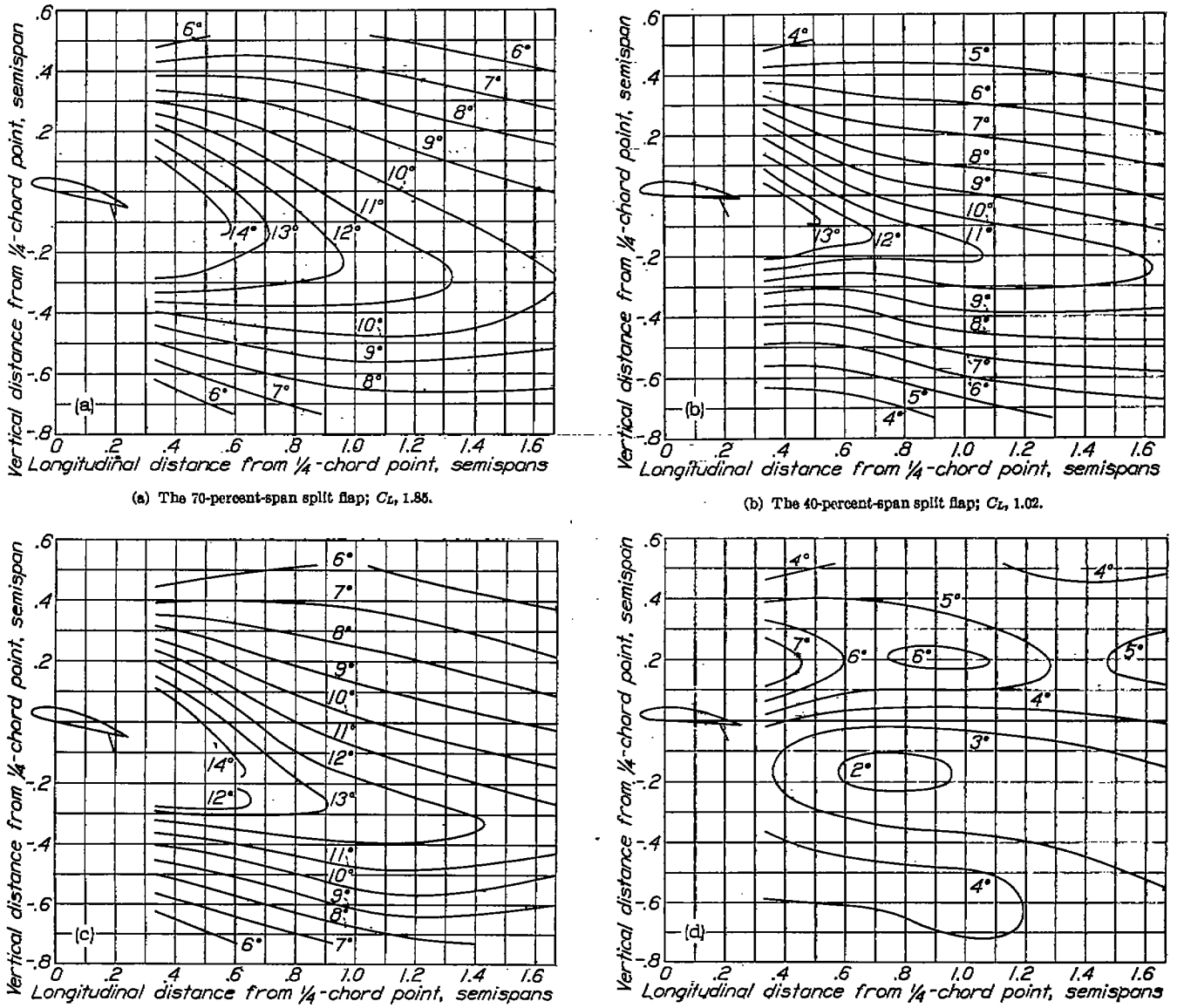

(a) The 70-percent-span split flap; C_L, 1.85.

(b) The 40-percent-span split flap; C_L, 1.02.

(c) The 40-percent-span split flap; C_L, 1.58.

d) The 70-percent-span split flap with 12.5-percent-span cutaway at center; C_L, 1.18.

FIGURE 31.—Downwash-angle contours in the symmetry plane behind the 2- by 12-foot Clark Y airfoil with partial-span split flaps at various lift coefficients. δ_f, 60°.

away would not be thoroughly distorted after a very short distance. This case is of less practical importance than might be supposed, because the added lift due to a flap appears to be carried across the fuselage even though the flaps themselves may end at the wing-fuselage juncture.

DOWNWASH BEHIND STALLED AIRFOILS

The matter of downwash behind stalled airfoils is of importance from considerations of stability and control at the stall. The available data for such cases are limited; hence an extensive treatment of the subject is not possible. A discussion based on that for unstalled airfoils and in agreement with the small amount of data available may, however, be useful.

The subject divides itself naturally into two parts, depending on whether the wing stalls at the tips or at the center. The effects of stalling on downwash fall roughly under two heads: (a) effects of the strong wake, and (b) effects of the change in the span load distribution.

For a wing stalled at the tips, the span load distribution may be compared with that for a wing with a partial-span flap as shown, for example, in figure 28, where the edge of the flap corresponds to the edge of the low-lift stalled region. The downwash in the region of the tail will therefore, for a given lift coefficient, be greater for the stalled wing than for the unstalled wing, because a substantial part of the vorticity that, for the unstalled wing, leaves the wing at the tip, now leaves at the edge of the stalled region.

An example of this effect will be noted when the mid-wing model is discussed. The wing being highly tapered, the stall in this case progresses inward from the tips. After the tips begin to stall, the lift remains nearly constant with increase in angle of attack and, correspondingly, so does the theoretical downwash (as computed for the unstalled wing). The experimental downwash, for the reason just given, continues to increase as the edge of the stalled region moves inward.

Wings with low taper ratio, or with washout, will stall first at the center. In addition to the change in the vortex distribution, corresponding to the change in

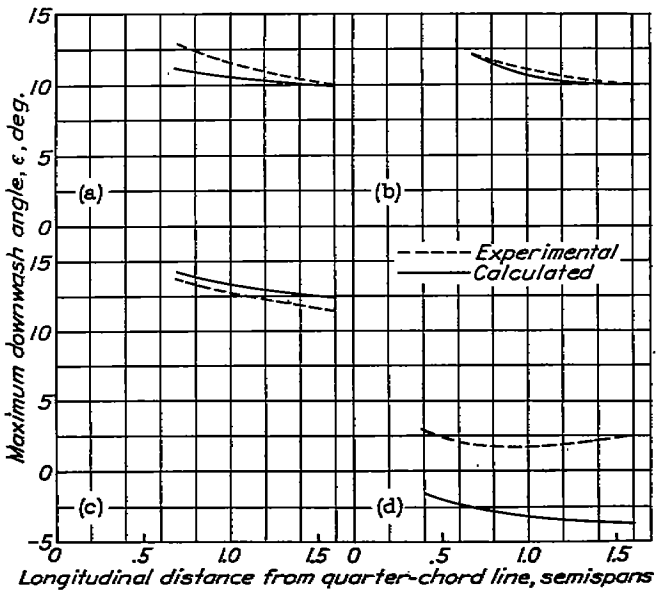

(a) The 70-percent-span split flap; C_L, 1.85.
(b) The 40-percent-span split flap; C_L, 1.02.
(c) The 40-percent-span split flap; C_L, 1.58.
(d) The 70-percent-span split flap with 12.5-percent-span cutaway at center; C_L, 1.18.

FIGURE 32.—Comparison of calculated and experimental downwash behind the 2- by 12-foot Clark Y airfoil with partial-span split flaps at various lift coefficients. δ_f, 60°.

span load distribution, the presence of the wake close to or passing over the tail is an important factor. The wake is very wide, but the position of its center can probably be predicted with fair accuracy from the span load distribution by the process previously described. As will be explained in a later section, the center of the wake leaves the wing, not at the trailing edge, but at a point about $(c/2)\sin\alpha$ above the trailing edge. In general, when a wing stalls at the center, the center of the wake moves upward. If the stall is gradual, this displacement will be small; if the lift drops sharply across the center of the wing, the vortices rolling off at the edge of the stalled portion will rotate in such a sense as to contribute an upward motion to the wake. The curve of figure 13 for the Clark Y airfoil at $\alpha=17.6°$ illustrates this effect. It will be seen that both the middle position of the wake and the mean downwash angle in the wake are approximately the same as for $\alpha=1.4°$, although the lift coefficient is three times as much. The figure also demonstrates the other characteristic of the air flow near a strong wake; namely, that, because of the flow of air into the wake, the downwash above it is increased, while that below it is decreased. The effect in this case amounts to about 3° or 4°.

WAKE

The wake may be defined as the region behind a wing in which the drag due to skin friction appears as a decreased total pressure. Bernoulli's equation does not apply within it, for there is a gradient in dynamic pressure, whereas the static pressure is almost constant. Owing to turbulent mixing at its boundaries, the wake widens with increasing distance downstream and at the same time becomes less intense. Far behind the wing, the wake becomes so thoroughly diffused with the surrounding stream that its presence can no longer be observed. Typical distributions of dynamic pressure in the wake are shown in figure 33.

Calculations for tail-surface design require a knowledge of the wake location, with reference to the tail, and of the wake dimensions. It will be shown that the wake location is dependent on the airfoil lift and that the wake dimensions are functions of the profile drag and essentially independent of the lift.

LOCATION OF THE WAKE

The wake behind a wing has been shown (figs. 8, 9, and 27) to coincide with the trailing vortex sheet. This coincidence is due to the common origin of the wake and the vortex sheet at or near the trailing edge of the wing and their equal freedom to move in the induced-velocity field behind the wing. It has previously been shown that the vertical displacement h of the vortex sheet from an origin at the trailing edge is given with satisfactory accuracy by

$$h=\int_{T.E.}^{x}\tan\epsilon\,dx$$

for the cases of wings without flaps at low and moderate lift coefficients. The necessity for an accurate knowledge of the vertical location of the wake requires that further consideration be given to the case of flapped wings and wings at lift coefficients at and above the stall.

Difficulties in determining the vertical location of the wake for the aforementioned cases arise, first, in establishing the vertical location of the origin of the wake at the trailing edge and, second, in evaluating the errors introduced by the assumptions made in computing the height of the vortex sheet. The simplified trailing-vortex system that has been shown to give satisfactory accuracy in downwash-angle computations may lead to somewhat larger errors in estimating the wake location.

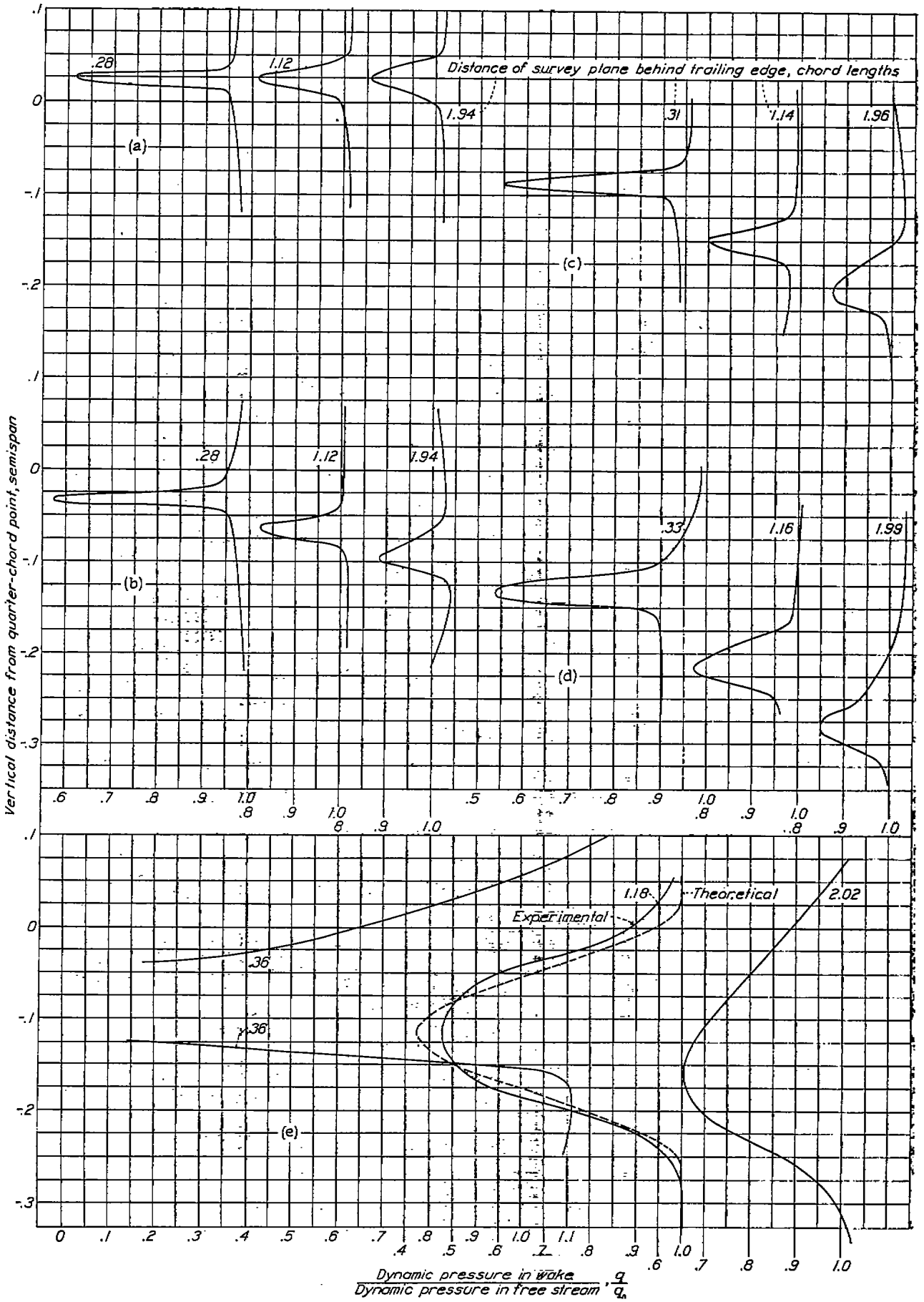

(a) $\alpha=-5.3°$; $C_L=0.08$. (b) $\alpha=1.6°$; $C_L=0.40$. (c) $\alpha=8.7°$; $C_L=0.90$. (d) $\alpha=15.2°$; $C_L=1.35$. (e) $\alpha=18.5°$; $C_L=1.00$ (stalled).

FIGURE 33.—Wake profiles showing dynamic pressure in the symmetry plane at three distances behind the U. S. A. 45 tapered airfoil at different lift coefficients.

From the experimental flap data available, it was not possible to isolate the discrepancies with the theory caused by improper choice of the wake origin from those due to the use of the simplified trailing-vortex system. It was therefore necessary to resort to an empirical method that fits the experimental data for full-span flaps with considerable accuracy. For the cases of partial-span flaps at high lifts, the wake will generally

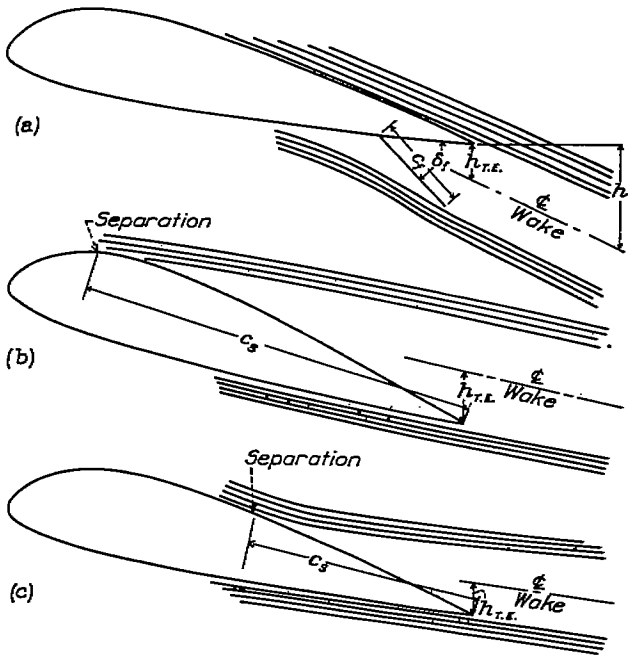

(a) A flapped airfoil.
(b) A completely stalled airfoil.
(c) A partly stalled airfoil.

FIGURE 34.—Streamlines illustrating the origin of the wake for flapped and stalled airfoils.

be slightly above the values given by the empirical expression.

For a wing with a deflected flap, it is apparent that the origin of the vortex sheet and the wake is below the original trailing edge of the wing. Inasmuch as the flow over the upper surface and that over the trailing edge of the deflected flap are separated by a distance equal to about $c_f \sin \delta_f$ (fig. 34), it was assumed as a first approximation that the wake has this thickness at the trailing edge with the center at a distance of $(c_f/2) \sin \delta_f$ below the original trailing edge. With this assumption of the position of the wake center and the further assumption that the wake was deflected behind the wing by an amount equal to $\int_{T.E.}^{x} \tan \epsilon \, dx$, a large number of comparisons were made with available experimental data on the wake location behind flapped wings. A systematic discrepancy between the theoretical and the experimental values was noted that was primarily a function of the flap deflection. The type of flap (split, plain, or external-airfoil) appeared to be of only secondary importance and has therefore been neglected. Values of k, which is the correction factor for the location of the wake origin at the trailing edge, are given in figure 35. Positive values of k indicate downward displacements.

The location of the wake origin behind a flapped wing with reference to the original (flap up) trailing edge of the wing is thus given as

$$h=(c_f/2) \sin \delta_f + kc + \int_{T.E.}^{x} \tan \epsilon \, dx$$

Owing to the relatively slow change in ϵ with distance behind the wing, a graphical integration of $\tan \epsilon \, dx$ may readily be performed. The values of ϵ are obtained from downwash-angle charts, such as figures 16 and 29.

When the wing stalls, the downwash at the wing center may be either increased or decreased depending on whether the wing stalls first at the tips or at the center. The center of the wake in the region of the trailing edge of a section is always raised, however, when the section either partly or completely stalls.

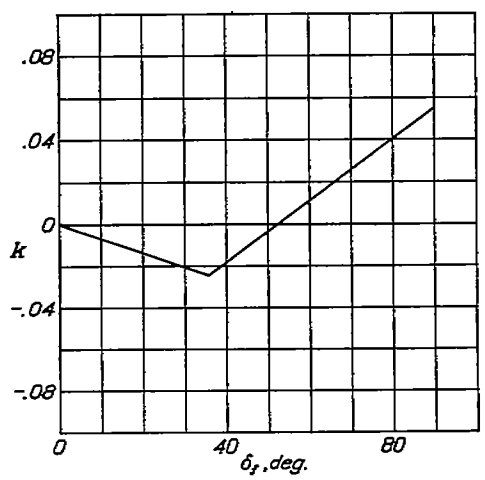

FIGURE 35.—Plot of factor k for correction to the vertical position of the wake origin at the trailing edge of a wing with a flap.

For cases in which the section is partly stalled (fig. 34 (c)) the wake center may be raised an amount equal to $(c_s/2) \sin \alpha$, in which c_s is the length of the wing chord over which the separation occurs. For a completely stalled wing, c_s approximately equals c. The foregoing approximations for location of the center of the wake with reference to the trailing edge of an unflapped wing have shown satisfactory agreement with the experimental data.

For the case of a flapped wing at the stall, the wake center will be raised above the trailing edge by an amount equal to $(c_s/2) \sin \alpha$ and, owing to the flap, will be lowered by an amount equal to $(c_f/2) \sin \delta_f$ so that the resultant displacement of the origin may be obtained as the algebraic sum of these two terms.

The wake displacement behind the wing depends directly on the downwash. It is not to be expected, therefore, that the wake location for a stalled wing may be predicted with great accuracy unless the exact nature of the stall is known and the change in the load distribution due to the stall is taken into account.

WAKE DIMENSIONS

The profile drag of an airfoil section may be approximately equated to the loss of momentum in the wake, as shown by Betz (reference 12) by the equation

$$d_0=\rho\int_{-\infty}^{\infty} u(U-u)\,dz$$

in which U is the velocity in the free stream and u is the local velocity in the wake. At distances behind the airfoil comparable with the tail-plane location where the static pressure in the wake has reached that of the free stream, the momentum equation may be approximated by the more elementary expression

$$c_{d_0}=\frac{1}{c}\int_{\frac{-B}{2}}^{\frac{B}{2}}\left(1-\frac{q}{q_0}\right)dz \qquad (2)$$

in which c_{d_0} is the section profile-drag coefficient, q/q_0 is the ratio of the dynamic pressure in the wake to that in the free stream, and B is the wake width. Experimental investigations have shown excellent agreement with this expression even for the cases of wings with flaps (reference 13).

The wake may be completely described by the width B, the loss of dynamic pressure at the wake center Δq, and the shape of the wake profile.

As an aid in generalizing the results, the following nondimensional ratios have been adopted:

$$\eta=\frac{\text{dynamic-pressure loss at center line of wake}}{\text{dynamic pressure in free stream}},\ \frac{\Delta q}{q_0}$$

$$=1-\frac{q}{q_0}$$

$$\zeta=\frac{1}{2}\frac{\text{wake width}}{\text{wing chord}},\ \frac{B}{2c}$$

$$\xi=\frac{\text{distance behind trailing edge of wing}}{\text{wing chord}},\ \frac{l}{c}$$

In a theoretical analysis of the wake behind a two-dimensional body, assuming the turbulent mixing length to be proportional to the wake width, Prandtl (reference 14) has indicated the following relations:

$$\zeta\propto\xi^{\frac{1}{2}}c_{d_0}^{\frac{1}{2}}$$

$$\eta\propto\frac{c_{d_0}^{\frac{1}{2}}}{\xi^{\frac{1}{2}}}$$

These proportionalities have been investigated by means of the experimental data. The wake widths for the three symmetrical airfoils at zero lift are plotted against distance from the wing trailing edge in figure 36. The curves are all parabolic, as indicated by the Prandtl expression. The origin is shifted to $\xi=-0.15$, which is to be expected, owing to the already finite boundary-layer width at the wing trailing edge. In figure 37 is shown the variation of the wake width 2ζ with c_{d_0} for a fixed value of ξ ($\xi\cong1.5$). The predicted proportionality with $c_{d_0}^{\frac{1}{2}}$ is verified, for the test points may be fitted to a parabola, the equation of which is $\zeta=0.89\,c_{d_0}^{\frac{1}{2}}$.

From the same test data, corresponding values of the relative losses in dynamic pressure at the wake center

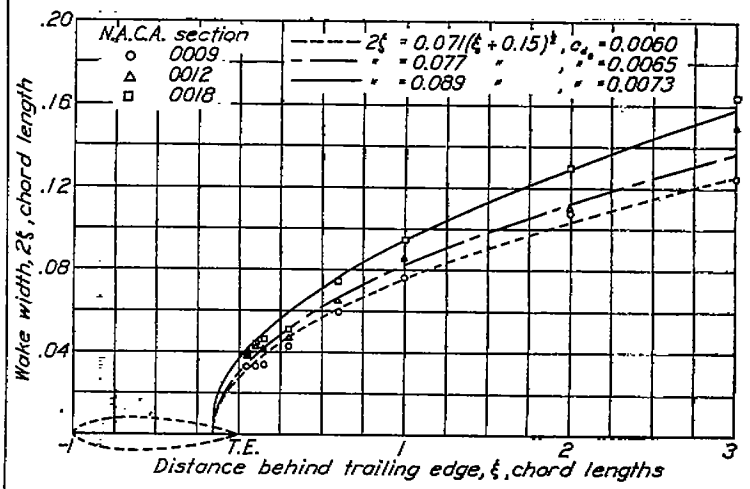

FIGURE 36.—Illustrations of parabolic relation between wake width and distance behind the trailing edge.

η are plotted against c_{d_0} (fig. 38); the predicted proportionality of η with $c_{d_0}^{\frac{1}{2}}$ is again substantiated. The variation in η with distance from the trailing edge is shown in figure 39 for the N. A. C. A. 0018 airfoil. In contrast to the Prandtl relation, the variation in this case appears to be with the inverse first power of ξ,

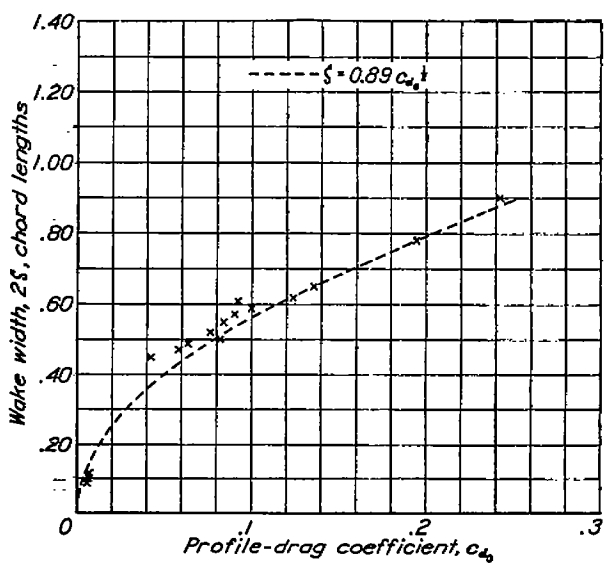

FIGURE 37.—Illustration of parabolic relation between wake width and profile drag. Distance behind trailing edge, ξ, 1.5 chord lengths. (Data from reference 13.)

rather than with the inverse ½ power. The discrepancy is doubtless associated with the high values of η near the trailing edge, for in Prandtl's discussion it was assumed that η is small. The inverse first power will be tentatively retained, although it is recognized that an obvious inconsistency exists for large values of ξ.

Applying the proportionality constants derived from the data leads to the equations

$$\eta=\frac{2.42\ c_{d_0}^{\frac{1}{2}}}{\xi+0.3} \tag{3}$$

$$\zeta=0.68\ c_{d_0}^{\frac{1}{2}}(\xi+0.15)^{\frac{1}{2}} \tag{4}$$

Curves representing these equations are plotted in figures 40 and 41. Combining (3) and (4) leads to the equation

$$\zeta/\eta=0.28(\xi+0.15)^{\frac{1}{2}}\ (\xi+0.3)$$

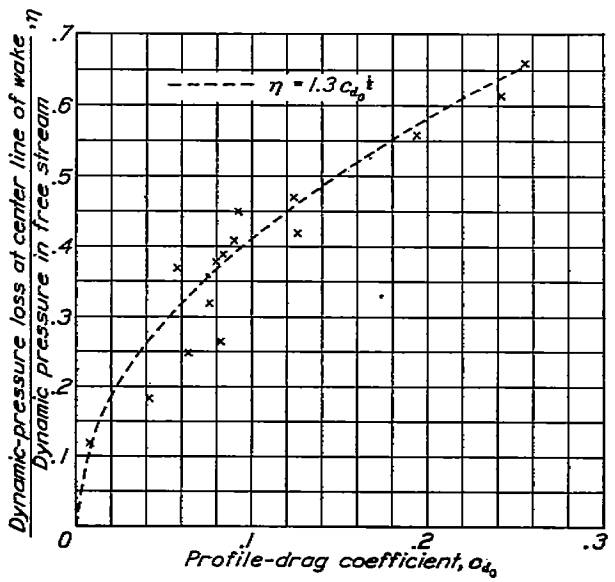

FIGURE 38.—Illustration of parabolic relation between maximum dynamic-pressure loss in wake and profile-drag coefficient. Distance behind trailing edge, ξ, 1.5 chord lengths. (Data from reference 13.)

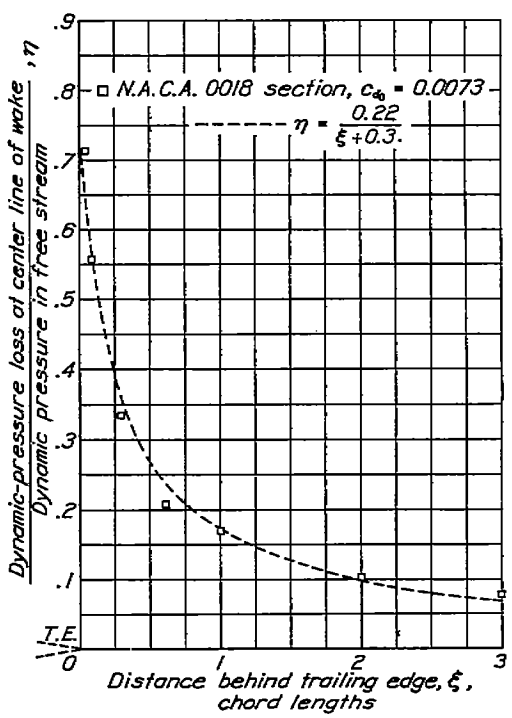

FIGURE 39.—Illustration of inverse relation between dynamic-pressure loss and distance behind the trailing edge for the N. A. C. A. 0018 airfoil.

The ratio of the wake width to the deficiency of dynamic pressure at the wake center is thus shown to be independent of the value of c_{d_0}.

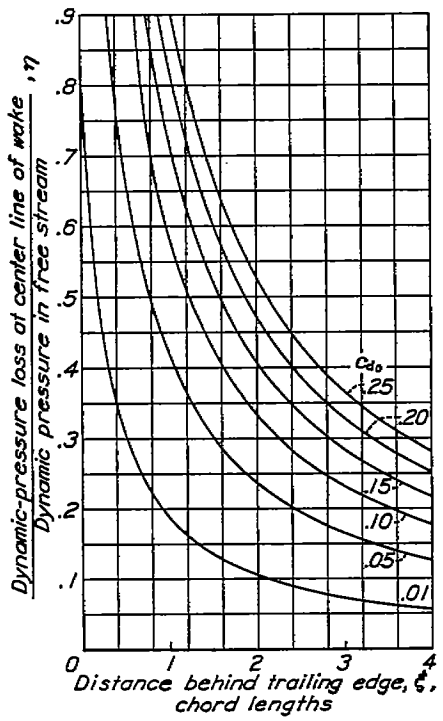

FIGURE 40.—Variation of maximum dynamic-pressure loss in the wake with distance behind the trailing edge.

$$\eta=\frac{2.42c_{d_0}^{\frac{1}{2}}}{\xi+0.3}$$

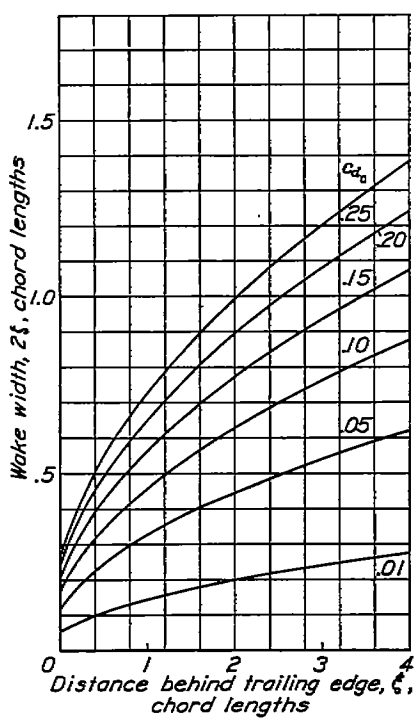

FIGURE 41.—Variation of wake width with distance behind the trailing edge.

$$\zeta=0.68c_{d_0}^{\frac{1}{2}}(\xi+0.15)^{\frac{1}{2}}$$

A complete description of the wake requires, in addition to ζ and η, the variation of the relative loss in dynamic pressure η' with the distance ζ' from the wake center line. The nondimensional wake profiles measured on the three symmetrical airfoils at different distances behind the trailing edge are shown in figure 42. Although the profiles vary somewhat, in the range of distances corresponding to the usual tail loca-

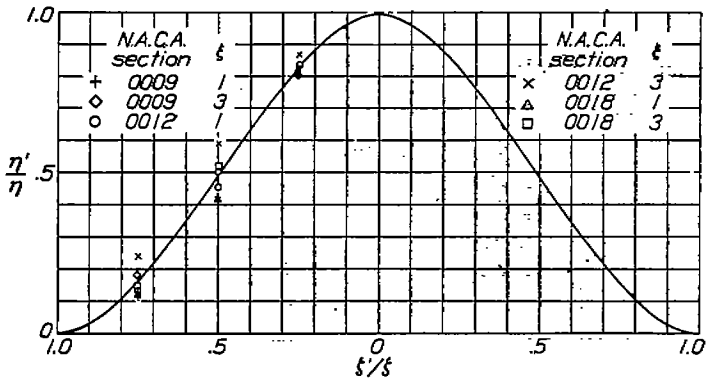

FIGURE 42.—Variation of dynamic-pressure loss across the wake.

$$\frac{\eta'}{\eta}=\left[1-\left(\frac{\zeta'}{\zeta}\right)^{1.75}\right]^2$$

tion the profile shape may be closely approximated by either of the following empirical equations:

$$\left.\begin{aligned}\frac{\eta'}{\eta}&=\left[1-\left(\frac{\zeta'}{\zeta}\right)^{1.75}\right]^2\\ \frac{\eta'}{\eta}&=\cos^2\frac{\pi\zeta'}{2\zeta}\end{aligned}\right\}\quad(5)$$

Equation (2) can be rewritten as

$$c_{d_0}=\int_{-\zeta}^{\zeta}\eta'd\zeta'$$

Substitution of values of η' from equation (5) and integration of the area under the wake profile provide the interesting result that

$$c_{d_0}\cong\eta\zeta \qquad (6)$$

An expression for c_{d_0} in terms of η and ζ may also be obtained from equations (3) and (4):

$$c_{d_0}=\frac{\eta\zeta(\xi+0.3)}{1.65(\xi+0.15)^{\frac{1}{2}}}=K_3\eta\zeta \qquad (7)$$

Values of K_3 from equation (7) are plotted against ξ in figure 43. The value of K_3 is unity at two chord lengths behind the airfoil; accordingly, only in this region are equations (6) and (7) in good agreement. The differences at the other values of ξ are attributed to the changing shape of the wake profiles with distance behind the airfoil and to the relative inaccuracy of equation (2) at small distances behind the wing.

Wake of stalled airfoils.—Although the empirical equations (3) and (4) for the wake dimensions were developed from results obtained at lifts below the stall, they apply with reasonable accuracy above the stall provided that the profile-drag coefficient of the stalled wing ahead of the particular region is known.

The rapid variation of c_{d_0} with C_L at the stall and the inexact knowledge of the profile-drag coefficients of stalled or partly stalled sections usually make an exact calculation difficult. When these data are available, satisfactory agreement is obtained, as shown by the comparison of the experimental and the predicted wake dimensions for the case of the stalled U. S. A. 45 airfoil in figure 33.

Interesting comparisons of the wake of the U. S. A. 45 airfoil at lift coefficients slightly above and below the stall can be obtained from a study of figures 44 to 47. The wake contours are marked in fractions of the free-stream dynamic pressure ($1-\eta'$) and results are given for surveys in planes at three longitudinal distances behind the airfoil and in the plane of symmetry of the airfoil.

It may be noted for the surveys at a longitudinal distance of 1.18 chord lengths (figs. 44 (b) and 45 (b)) behind the trailing edge of the wing, which most nearly

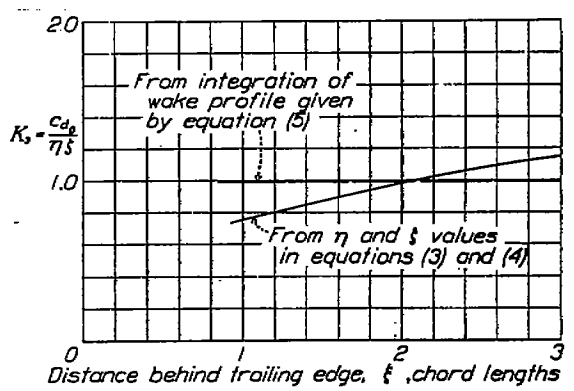

FIGURE 43.—Relation between profile-drag coefficient and the product of wake half width by maximum dynamic-pressure loss.

corresponds to the usual tail location, that the dynamic pressure in the plane of symmetry of the wing and at the wake center line changes from 0.8 q_0 for the unstalled condition to 0.5 q_0 at several degrees above the stall. The value of η is therefore increased from 0.2 to 0.5. The corresponding profile-drag coefficients for the unstalled and the stalled conditions are 0.018 and 0.130, respectively (reference 1).

Since $\eta \propto c_{d_0}^{\frac{1}{2}}$, it may be expected that

$$\frac{\eta_{stalled}}{\eta_{unstalled}} \text{ and } \frac{c_{d_0}^{\frac{1}{2}}{}_{stalled}}{c_{d_0}^{\frac{1}{2}}{}_{unstalled}} \text{ should be equal.}$$

A fairly satisfactory agreement is found; thus, upon substitution of the numerical values, the first ratio gives 2.5 and the second gives 2.7.

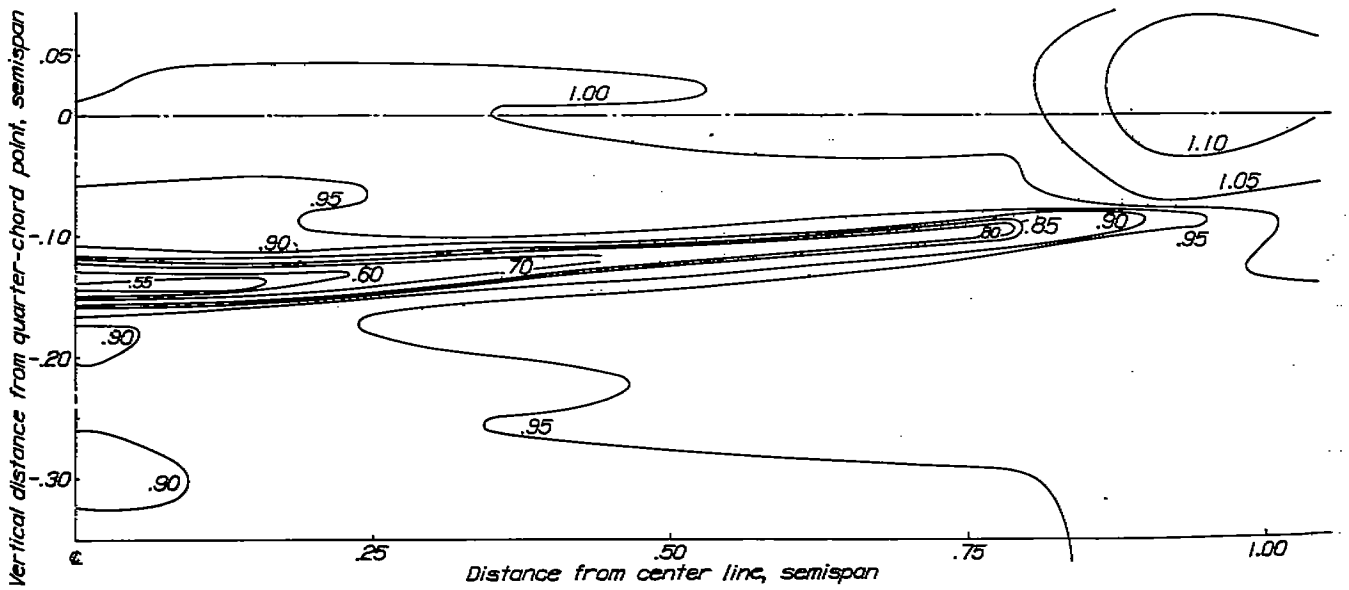

(a) Plane 0.33c behind the trailing edge.

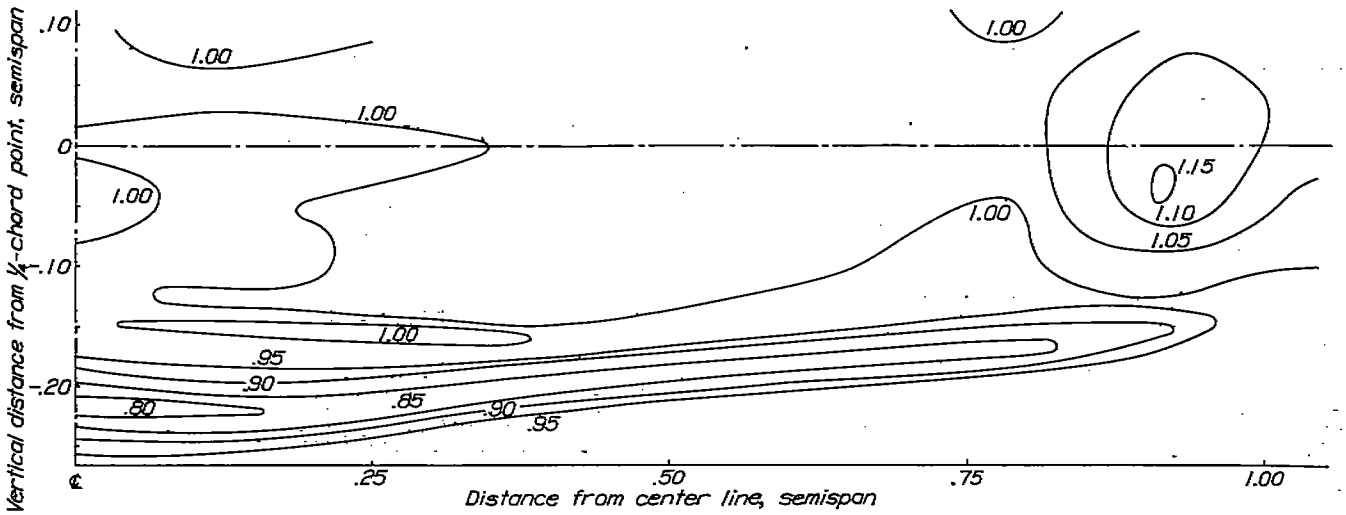

(b) Plane 1.18c behind the trailing edge.

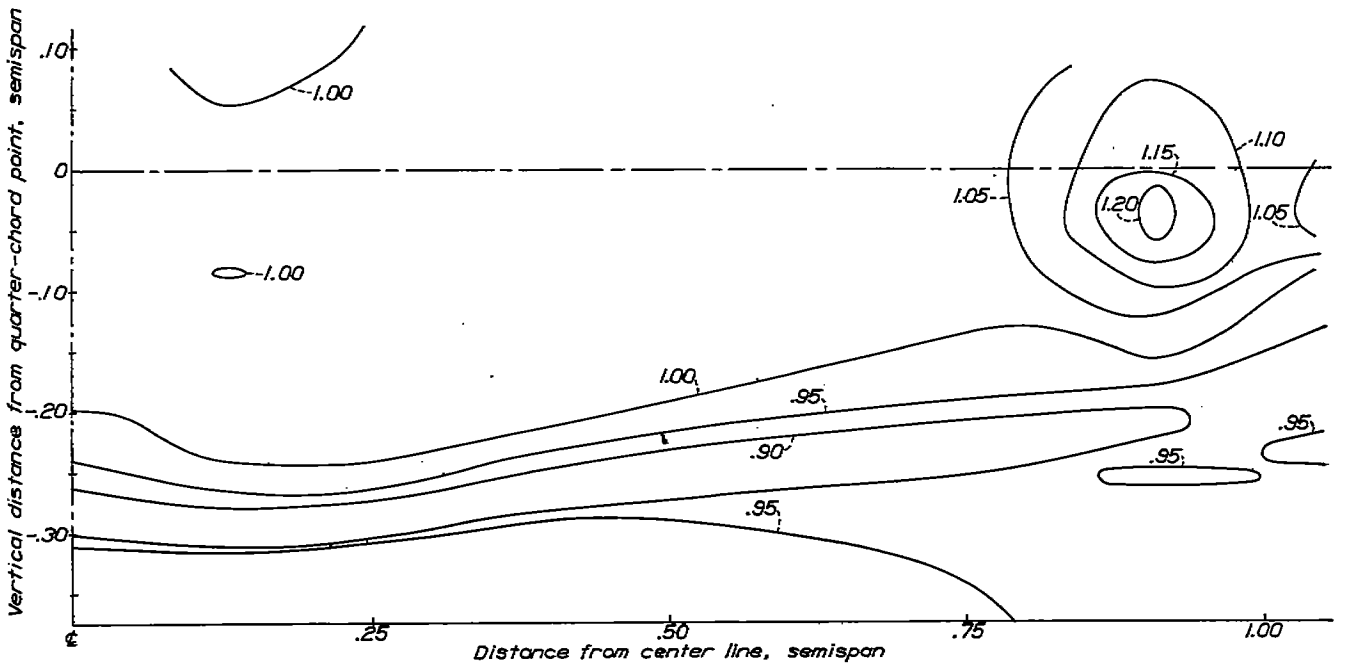

(c) Plane 1.99c behind the trailing edge.

FIGURE 44.—Contour lines of dynamic pressure in planes parallel to the span and various distances behind the trailing edge of the center section of the U. S. A. 45 tapered airfoil. Dynamic pressures in fractions of free-stream dynamic pressure; α, 15.2°; C_L, 1.35.

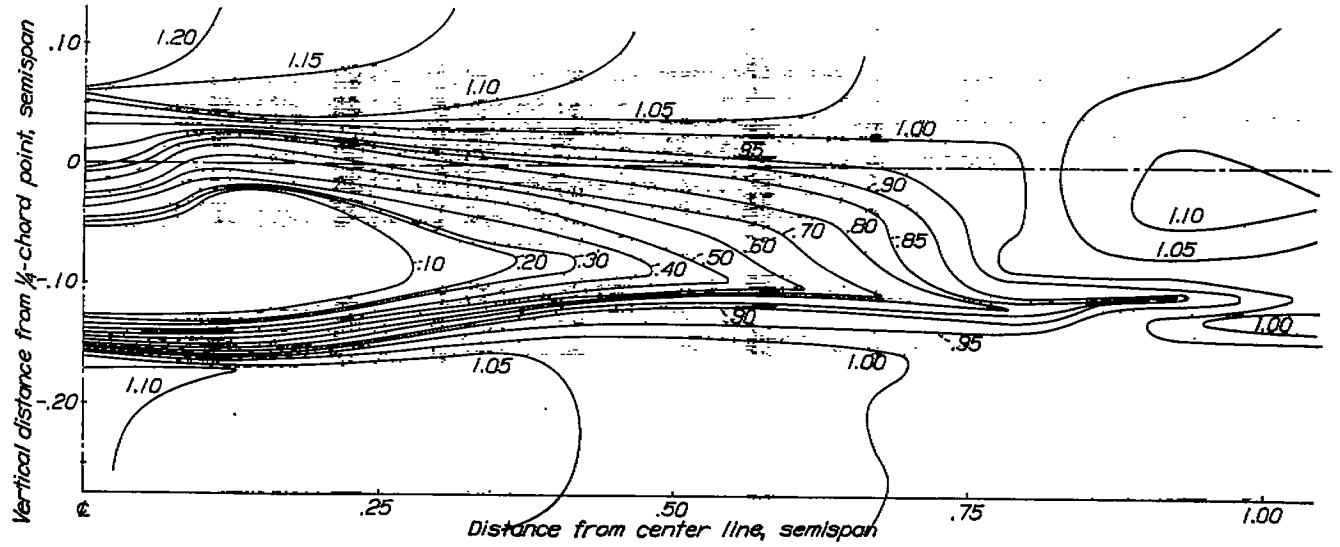

(a) Plane 0.36c behind the trailing edge.

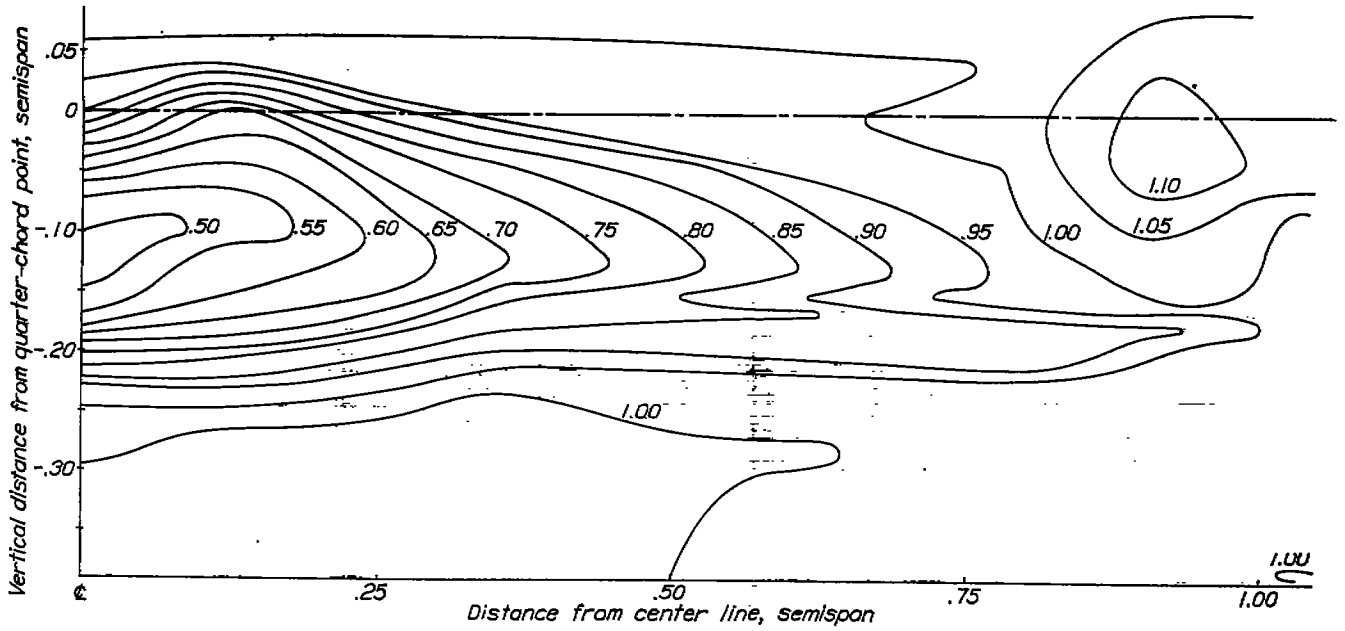

(b) Plane 1.18c behind the trailing edge.

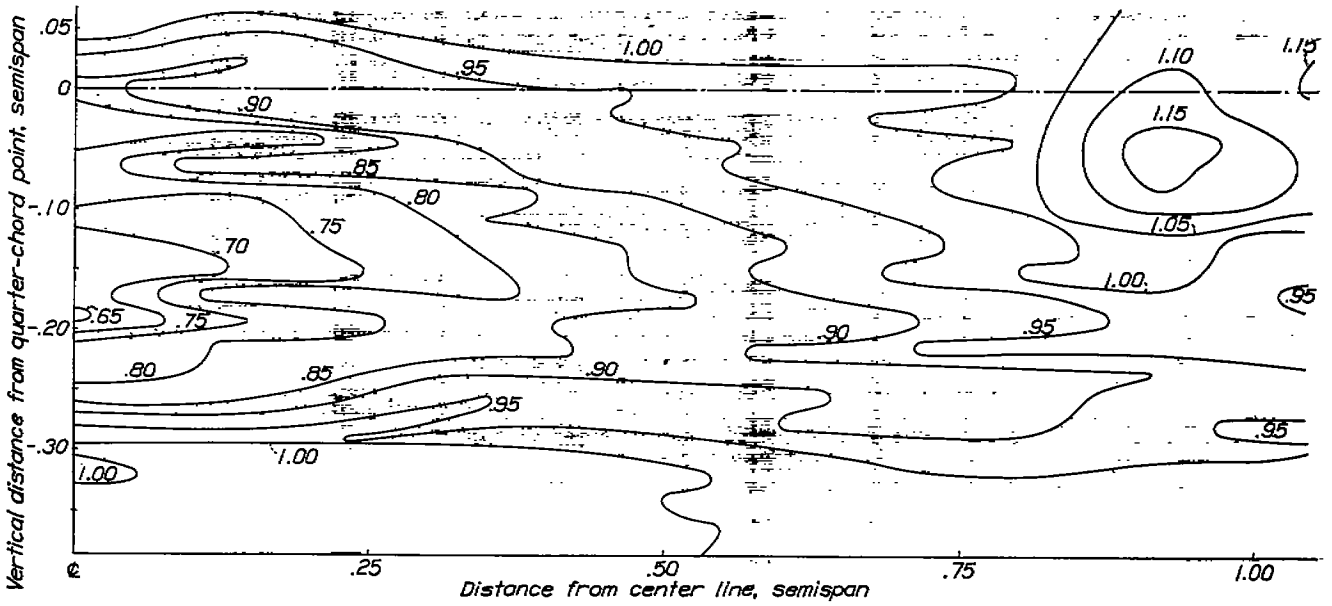

(c) Plane 2.02c behind the trailing edge.

FIGURE 45.—Contour lines of dynamic pressure in planes parallel to the span and various distances behind the trailing edge of the center section of the U. S. A. 45 tapered airfoil. Dynamic pressures in fractions of free-stream dynamic pressure; airfoil stalled; α, 18.5°; C_L, 1.00.

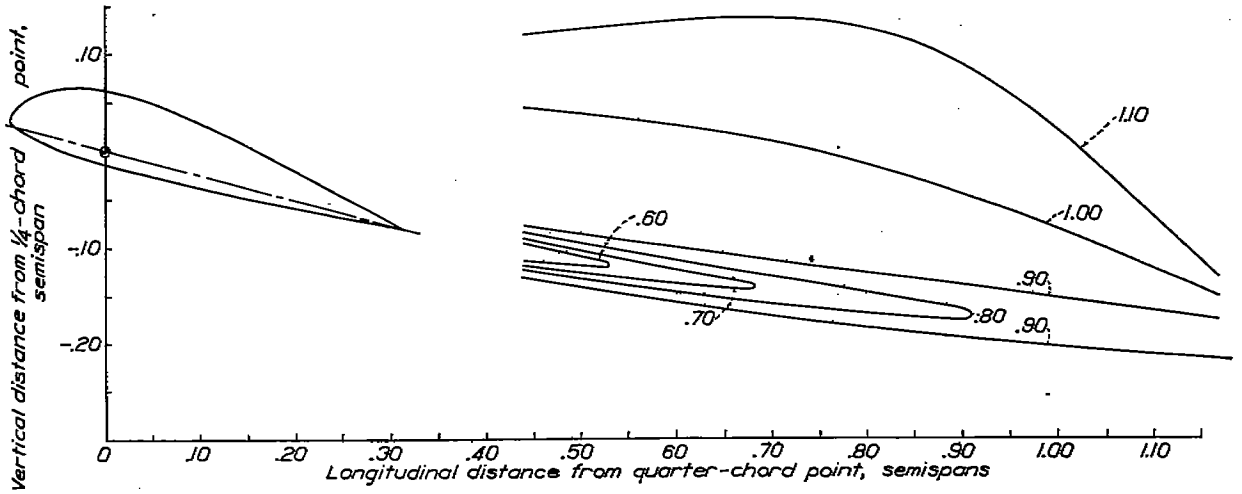

FIGURE 46.—Contour lines of dynamic pressure in the symmetry plane behind the U. S. A. 45 tapered airfoil. Dynamic pressures in fractions of free-stream dynamic pressure; α, 15.2°; C_L, 1.35.

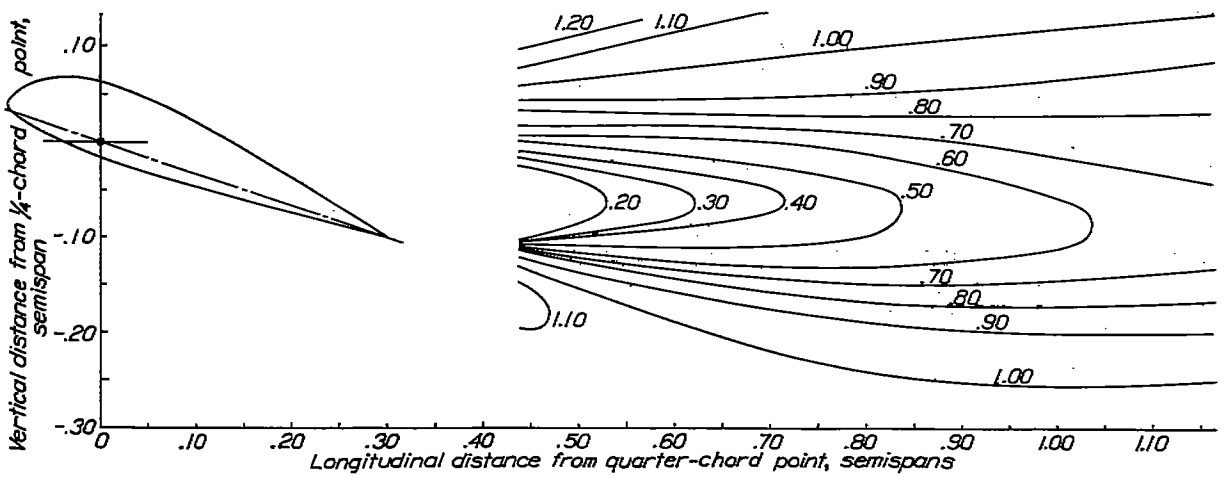

FIGURE 47.—Contour lines of dynamic pressure in the symmetry plane behind the U. S. A. 45 tapered airfoil. Dynamic pressures in fractions of free-stream dynamic pressure; airfoil stalled; α, 18.5°; C_L, 1.00.

Calculation of the wake effect on downwash angle.—From the equation $\eta'=\eta\cos^2\frac{\pi\zeta'}{2\zeta}$ and the definition of η',

$$\eta'=1-\frac{V^2}{V_0^2}$$

it follows that the velocity V at a point (ξ, ζ) in the wake is given by

$$\frac{V}{V_0}=\sqrt{1-\eta\cos^2\frac{\pi\zeta'}{2\zeta}}$$

The flow (in two dimensions) passing between a point $(\xi, 0)$ on the wake center and the point distant ζ' above it (ξ, ζ'), is

$$\psi=c\int_0^{\zeta'} V d\zeta'=cV_0\int_0^{\zeta'}\sqrt{1-\eta\cos^2\frac{\pi\zeta'}{2\zeta}}d\zeta'$$

in which η and ζ' are functions of c_{d_0} and ξ. The stream function ψ can be evaluated from tables of elliptic integrals; for a particular pair of values of c_{d_0} and ξ, it is a function of ζ'. After this function has been computed for different values of ξ, streamlines may be drawn, for they are loci of points for which the values of ψ are constant. The inclination of the streamline passing through any point is the wake effect on the downwash angle at that point.

The calculation, as here described, applies for points lying within the wake ($\zeta'/\zeta \leqq 1$). The effect diminishes with distance from the edge of the wake. Inasmuch as the tail plane is not usually very far from the wake, the effect at the tail may be considered equal to that at the wake edge near it. Figure 48 shows the results of the calculations for $c_{d_0}=0.1$ and 0.2, for $\xi=1.5$, which corresponds approximately to the usual longi-

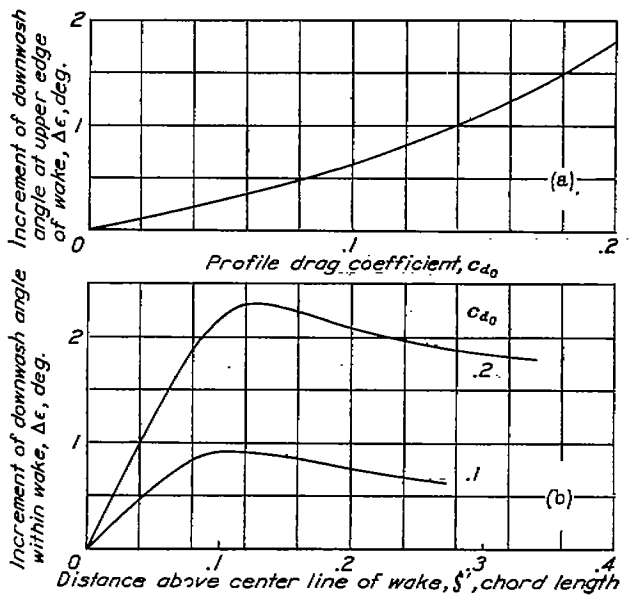

(a) Variation with profile-drag coefficient.
(b) Variation with distance above wake center line.

FIGURE 48.—Effect of wake on downwash at 1.5 chord lengths behind the trailing edge.

tudinal location of the tail plane. At much higher drag coefficients, the effect becomes so large that it is not possible to predict, with any accuracy, the downwash in the wake behind completely stalled airfoils. An example may be seen in the surveys behind the stalled low-wing monoplane with flaps down (fig. 22(a)); the profile-drag coefficient of the stalled section is about 0.5, and the maximum effect on the downwash angle is about 15°.

APPLICATION TO AN AIRPLANE

In order to show the application of the method, it will be applied to the case of the typical midwing-monoplane model, for which experimental data are available for comparison.

The calculations are based on the theoretical span load distributions of figure 49. For convenience, the curve for the plain wing is shown for $C_{L_w}=1.00$ and that for the flap is for $C_{L_f}=0.64$. Figure 50 indicates the progress of the calculation for the case of flaps up, at $C_L=1.1$. The downwash-angle contours are shown first undisplaced and then displaced in the manner previously discussed, so that the center line passes through the trailing edge and follows the downflow. For purposes of comparison with pitching-moment results, a correction factor of 0.95 should be applied in order to obtain the average value along the span of the tail. Incidentally, it may be noted that this center line and the wake center line which coincides with it fall below

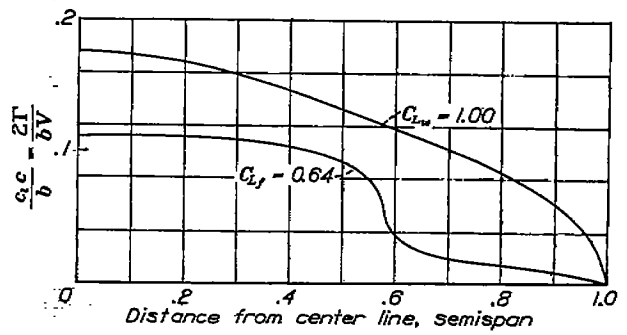

FIGURE 49.—Contributions of plain wing and of flap to the span load distribution for the midwing-monoplane model.

the tail and that the wake as computed by equation (4) does not flow over the tail.

Steps in the calculation for a case of the airplane with flaps down appear in figure 51. The undisplaced downwash-angle contours corresponding to the plain wing ($C_{L_w}=0.96$) are shown as well as the contribution of the

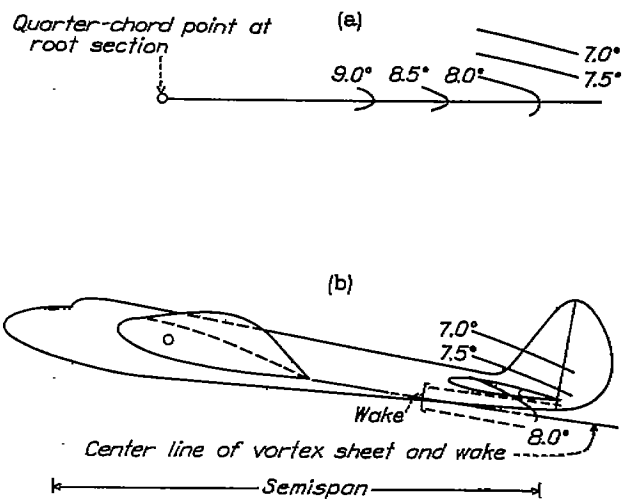

(a) Undisplaced pattern.
(b) Pattern displaced so that center line passes through the trailing edge and follows the downflow.

FIGURE 50.—Theoretical downwash-angle contours and wake location for the midwing-monoplane model. Flaps up; C_L, 1.1.

flap ($C_{L_f}=0.64$). Addition of these two contour maps leads to the contours shown in figure 51 (c). When the center line is so displaced that it passes through the wake origin, which in this case is just below the middle of the flap opening (see fig. 35), and follows the downflow, the contours of figure 51 (d) are obtained. The edge of the wake, as found by equation (4), again falls below the tail.

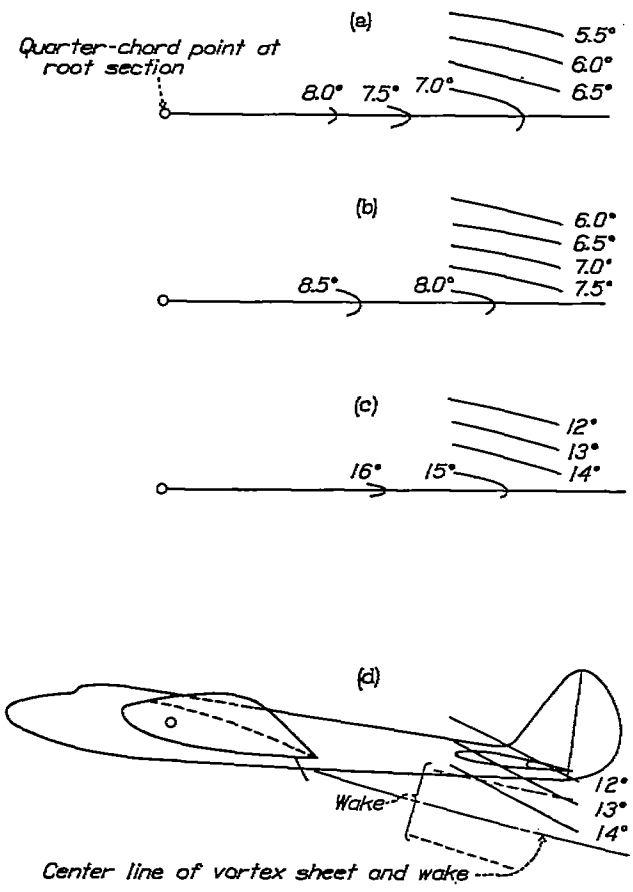

(a) Contribution of plain wing.
(b) Contribution of flap.
(c) Total calculated downwash, (a)+(b), undisplaced.
(d) Pattern displaced so that center line passes through the wake origin and follows the downflow.

FIGURE 51.—Theoretical downwash-angle contours and wake location for the midwing-monoplane model. Flaps down; C_{L_w}, 0.96; C_{L_f}, 0.64

The downwash angles so obtained should, for purposes of comparison with pitching-moment measurements, be corrected by a factor of 0.9 in order to get the average value along the span of the tail and by an increment of 0.5°, which is the estimated effect of the wake.

Experimental values of the downwash angles were obtained by comparing tail-off pitching moments with tail-on pitching moments obtained at different stabilizer settings. The stabilizer settings corresponding to zero load on the tail are found by interpolation or extrapolation. From these values, the corresponding angles of attack of the airplane, and the jet-boundary corrections (reference 4), the downwash angles are derived. The agreement between theory and experiment is shown in figure 52 to be satisfactory, except at the higher angles of attack, where the tips are stalled.

This case may be considered a particularly favorable one, for the model was well streamlined and had a relatively small fuselage. It is likely, however, that, as in the present example, interference will be small in modern carefully streamlined airplanes.

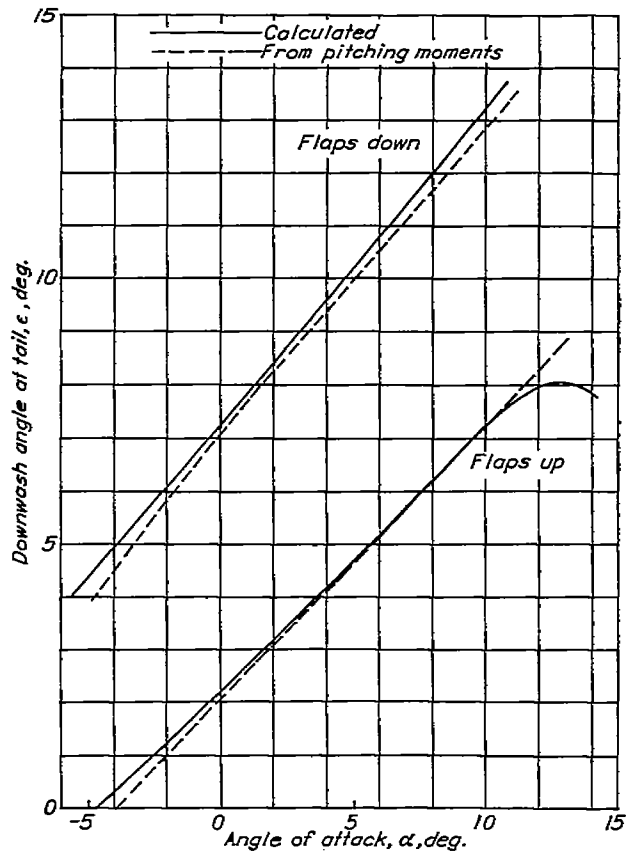

FIGURE 52.—Comparison of calculated and experimental downwash at the tail of the midwing-monoplane model.

CONCLUSIONS

1. The Biot-Savart equation, the theoretical span load distribution, and the lifting-line concept provide a sufficient basis for computation of the downwash angle behind airfoils with and without flaps.

2. The concentration of the trailing vortex sheet into a single pair of trailing vortices may be neglected for purposes of downwash computations.

3. The potential flow about an airfoil section is closely approximated by that about a vortex at its lifting line, for distances greater than one chord from the airfoil trailing edge.

4. The vertical displacement of the trailing vortex sheet due to the downflow must be taken into account in the calculations.

5. The loss in dynamic pressure at the wake center is directly proportional to the square root of the profile-drag coefficient and inversely proportional to the distance behind the airfoil trailing edge.

6. The wake width is directly proportional to the square root of the product of the profile-drag coefficient and the distance behind the airfoil.

7. The wake profile may be accurately given by an empirical expression involving as parameters only the wake width and the loss in dynamic pressure at the wake center.

8. The wake parameters are relatively independent of the airfoil lift, and the relations for the unstalled airfoil apply with almost equal accuracy above the stall.

LANGLEY MEMORIAL AERONAUTICAL LABORATORY,
NATIONAL ADVISORY COMMITTEE FOR AERONAUTICS,
LANGLEY FIELD, VA., *June 23, 1938.*

REFERENCES

1. Parsons, John F.: Full-Scale Force and Pressure-Distribution Tests on a Tapered U. S. A. 45 Airfoil. T. N. No. 521, N. A. C. A., 1935.
2. Silverstein, Abe: Scale Effect on Clark Y Airfoil Characteristics from N. A. C. A. Full-Scale Wind-Tunnel Tests. T. R. No. 502, N. A. C. A., 1934.
3. DeFrance, Smith J.: The N. A. C. A. Full-Scale Wind Tunnel. T. R. No. 459, N. A. C. A., 1933.
4. Silverstein, Abe, and Katzoff, S.: Experimental Investigation of Wind-Tunnel Interference on the Downwash behind an Airfoil. T. R. No. 609, N. A. C. A., 1937.
5. Silverstein, Abe, and Katzoff, S.: Design Charts for Predicting Downwash Angles and Wake Characteristics behind Plain and Flapped Wings. T. R. No. 648, N. A. C. A., 1939.
6. Theodorsen, Theodore: Theory of Wing Sections of Arbitrary Shape. T. R. No. 411, N. A. C. A., 1931.
7. Kaden, H.: Aufwicklung einer unstabilen Unstetigkeitsfläche. Ingenieur-Archiv, II Band, no. 2, May 1931, S. 140–168.
8. Muttray H.: Investigations on the Amount of Downwash behind Rectangular and Elliptical Wings. T. M. No. 787, N. A. C. A., 1936.
9. Glauert, H.: The Elements of Aerofoil and Airscrew Theory. Cambridge University Press, 1926, p. 138.
10. Lotz, Irmgard: Berechnung der Auftriebsverteilung beliebig geformter Flügel. Z. F. M., 22. Jahrg., 7. Heft, 14. April 1931, S. 189–195.
11. Pearson, H. A.: Span Load Distribution for Tapered Wings with Partial-Span Flaps. T. R. No. 585, N. A. C. A., 1937.
12. Betz, A.: A Method for the Direct Determination of Wing-Section Drag. T. M. No. 337, N. A. C. A., 1925.
13. Clark, K. W., and Kirkby, F. W.: Wind Tunnel Tests of the Characteristics of Wing Flaps and Their Wakes. R. & M. No. 1698, British A. R. C., 1936.
14. Prandtl, L.: The Mechanics of Viscous Fluids. Spread of Turbulence. Vol. III, div. G, sec. 25 of Aerodynamic Theory, W. F. Durand, ed., Julius Springer (Berlin), 1935, p. 165.